Metabolic Engineering 80 (2023) 45–65

Contents lists available at ScienceDirect

Metabolic Engineering

journal homepage: www.elsevier.com/locate/meteng

Multi-omics view of recombinant *Yarrowia lipolytica*: Enhanced ketogenic amino acid catabolism increases polyketide-synthase-driven docosahexaenoic production to high selectivity at the gram scale

Sofija Jovanovic Gasovic, Demian Dietrich, Lars Gläser, Peng Cao, Michael Kohlstedt, Christoph Wittmann *

Institute of Systems Biotechnology, Saarland University, Germany

ARTICLE INFO

Keywords:
PUFA
Omega-3 fatty acid
Docosahexaenoic acid
DHA
Yarrowia lipolytica
Fatty acid
CoA thioester
Acetyl-CoA
Malonyl-CoA
PKS synthase
Glycerol
Ketogenic amino acid
Transcriptome
Metabolome
Fluxome
13C
Systems biology
Multi-omics
Polyketide
Lipid

ABSTRACT

DHA is a marine PUFA of commercial value, given its multiple health benefits. The worldwide emerging shortage in DHA supply has increased interest in microbial cell factories that can provide the compound *de novo*. In this regard, the present work aimed to improve DHA production in the oleaginous yeast strain *Y. lipolytica* Af4, which synthetized the PUFA *via* a heterologous myxobacterial polyketide synthase (PKS)-like gene cluster. As starting point, we used transcriptomics, metabolomics, and ^{13}C-based metabolic pathway profiling to study the cellular dynamics of *Y. lipolytica* Af4. The shift from the growth to the stationary DHA-production phase was associated with fundamental changes in carbon core metabolism, including a strong upregulation of the PUFA gene cluster, as well as an increase in citrate and fatty acid degradation. At the same time, the intracellular levels of the two DHA precursors acetyl-CoA and malonyl-CoA dropped by up to 98% into the picomolar range. Interestingly, the degradation pathways for the ketogenic amino acids L-lysine, L-leucine, and L-isoleucine were transcriptionally activated, presumably to provide extra acetyl-CoA. Supplementation with small amounts of these amino acids at the beginning of the DHA production phase beneficially increased the intracellular CoA-ester pools and boosted the DHA titer by almost 40%. Isotopic ^{13}C-tracer studies revealed that the supplements were efficiently directed toward intracellular CoA-esters and DHA. Hereby, L-lysine was found to be most efficient, as it enabled long-term activation, due to storage within the vacuole and continuous breakdown. The novel strategy enabled DHA production in *Y. lipolytica* at the gram scale for the first time. DHA was produced at a high selectivity (27% of total fatty acids) and free of the structurally similar PUFA DPA, which facilitates purification for high-value medical applications that require API-grade DHA. The assembled multi-omics picture of the central metabolism of *Y. lipolytica* provides valuable insights into this important yeast. Beyond our work, the enhanced catabolism of ketogenic amino acids seems promising for the overproduction of other compounds in *Y. lipolytica*, whose synthesis is limited by the availability of CoA ester precursors.

1. Introduction

Docosahexaenoic acid (DHA, C22:6) is a polyunsaturated omega-3 fatty acid (PUFA) with recognized commercial value (Jovanovic et al., 2021). The compound supports fetal development (Valenzuela and Nieto, 2001), as well as neuronal (Sun et al., 2018a), retinal (Mun et al., 2019), and immune function (Calder, 2018), protects cardiovascular function (Swanson et al., 2012) and is crucial for protecting against inflammation (Zhang et al., 2019), peripheral artery disease, major coronary events and anticoagulation (Yanai et al., 2018). Furthermore, people with high DHA content have a significantly reduced risk of Alzheimer's disease (Cardoso et al., 2016). However, our body can only synthesize a small amount of DHA from other fatty acids, so we need to consume PUFAs directly from food supplements (Castro et al., 2016; Kabeya et al., 2018). Traditionally, the food-based intake of DHA mainly relies on marine oily fish such as salmon, sardine, herring, and mackerel that feed on marine phytoplankton as primary producers of this PUFA (Emery et al., 2016). Unfortunately, the supply of marine PUFAs from the oceans is tremendously declining because of overfishing (Hicks et al., 2019), climate warming (Hixson and Arts, 2016), and pollution

* Corresponding author.
E-mail address: christoph.wittmann@uni-saarland.de (C. Wittmann).

https://doi.org/10.1016/j.ymben.2023.09.003
Received 26 May 2023; Received in revised form 4 September 2023; Accepted 4 September 2023
Available online 7 September 2023

(Lundebye et al., 2017). Aqua-cultured fish do not offer a solution because fish farming requires supplementation with DHA itself. Long-term predictions suggest a severe shortage of DHA, where more than 90% of the world's population will be DHA-deprived due to the drastically decline in DHA content in fish by 2100 (Colombo et al., 2020). In addition, DHA receives huge interest for medical treatment, involving its use as high purity active pharmaceutical ingredient (API). The ClinicalTrials.gov database presently lists more than 400 clinical trials up to stage 4 related to DHA (https://www.clinicaltrials.gov).

In this regard, microbial cell factories offer a promising sustainable route to satisfy the future DHA demand (Ji and Huang, 2019). In addition to native microbes such as *Schizochytrium* sp. (Kujawska et al., 2021; Sahin et al., 2018), *Aurantiochytrium* sp. (Heggeset et al., 2019; Bartosova et al., 2021; Hussain et al., 2021; Nazir et al., 2018) and *Crypthecodinium cohnii* (Pei et al., 2017), oleaginous yeasts have emerged as promising heterologous PUFA producers (Jovanovic et al., 2021). Among these, *Yarrowia lipolytica*, an unconventional lipid-accumulating dimorphic yeast (Barth, 2013), has demonstrated its value in proof-of-concept studies (Thevenieau et al., 2007) focused on synthetizing lipids (Papanikolaou and Aggelis, 2003) and different PUFAs up to 20 carbon atoms in length, including linoleic acid (CLA, C18:2) (Imatoukene et al., 2017), α-linolenic acid (ALA, C18:3) (Cordova and Alper, 2018), arachidonic acid (ARA, C20:4) (Liu et al., 2019b), and eicosapentaenoic acid (EPA, C20:5) (Xue et al., 2013), Hereby, the PUFAs were synthetized through the native fatty acid biosynthetic pathway and introduced elongases and desaturases. In addition, we recently reported the overproduction of DHA in recombinant *Y. lipolytica* Af4 (Gemperlein et al., 2019) using a heterologous PUFA synthase from a myxobacterium that offered a reduced NADPH demand for product synthesis (Gemperlein et al., 2019). In a fed-batch process, *Y. lipolytica* Af4 produced 300 mg L^{-1} DHA from glycerol, whereby the cells went through different growth stages.

Here, we studied the glycerol-grown DHA producer Af4 in batch cultures at the system level. Time-resolved q-RT-PCR analysis of selected key genes involved in DHA synthesis and fatty acid metabolism revealed fundamental changes during the production process. Surprisingly, the intracellular pools of acetyl-CoA and malonyl-CoA, the two DHA precursors, dropped by up to 98% into the picomolar range at the onset of production. Global transcription profiling then provided a detailed view of the dynamics of the metabolic carbon core machinery. The observed dynamic pattern was highly similar for different nutrient regimes. Interestingly, catabolic pathways of ketogenic amino acids were found to be strongly upregulated in all cases when cells entered the stationary phase, which contributed to the supply of CoA precursors. Feeding small amounts of L-lysine, L-leucine, and L-isoleucine during this phase increased the pools of acetyl-CoA and malonyl-CoA, which boosted the production of DHA up to 40% and markedly increased product selectivity. Supplementation with citrate, also known to generate acetyl-CoA during breakdown, increased the DHA titer as well, but to a lesser extent and did not improve selectivity. Using ^{13}C isotope experiments, we further demonstrated that significant fractions of carbon from the added ketogenic amino acids were incorporated into intracellular amino acids, CoA esters, and DHA. L-Lysine appeared most valuable because cells seemed to transiently store it in the vacuole, providing a long-term effect over several days. In a fed-batch process with supplemented pulses of L-lysine, *Y. lipolytica* Af4 produced DHA at the gram scale, threefold more than what has been previously achieved, providing an important next step toward industrial production of this commercially attractive PUFA.

2. Materials and methods

2.1. Strains

The uracil-auxotrophic yeast *Y. lipolytica* Po1h (CLIB 882) and its prototrophic DHA-producing derivative Po1hSynPfaPptAf4, which expressed a myxobacterial PUFA synthase and a phosphopantetheinyl transferase (PPTase) from the myxobacterium *A. fasciculatus* (SBSr002), were obtained from previous work (Gemperlein et al., 2019).

2.2. Growth and DHA production medium

Different media were used to grow *Y. lipolytica*. Complex YPD medium contained 20 g L^{-1} of glucose, 20 g L^{-1} of peptone (Becton Dickinson, Heidelberg, Germany), and 10 g L^{-1} of yeast extract (Sigma Aldrich, Saint Louis, MO, USA). For YPD plate cultures, 20 g L^{-1} of agar was added (Becton & Dickinson). In addition, minimal YNB medium was used. In its basic composition, it contained 10 g L^{-1} of glycerol, 5 g L^{-1} of (NH4)2SO4, and 1.7 g L^{-1} of yeast nitrogen base (YNB, without amino acids and $(NH_4)_2SO_4$, Sigma Aldrich) in 200 mM MES buffer (pH 6.8). As specified below, the medium formulation was modified as follows throughout this work: (i) replacement of glycerol by glucose, (ii) increased glycerol level, (iii) varied carbon-to-nitrogen (C/N) ratio, and (iv) varied carbon-to-phosphorous (C/P) ratio. In further studies, the medium was supplemented with citrate (10 mM and 20 mM), L-lysine (10 mM), L-leucine (10 mM), and L-isoleucine (10 mM), respectively, at the beginning of the stationary phase. In isotopic tracer studies, ^{13}C-enriched supplements were added instead: 10 mM 99% [$^{13}C_6$] citrate (Sigma Aldrich), 10 mM 99% [$^{13}C_6$] L-lysine (Cambridge Isotope Laboratories, Andover, MA, USA), and 10 mM 99% [$^{13}C_6$] L-leucine (Cambridge Isotope Laboratories). In further experiments, we showed that the replacement of YNB with a homemade synthetic mixture of the corresponding vitamins and trace metals did not affect the cultures. When growing the wild type cultures, 50 mg L^{-1} uracil was added to the medium.

2.3. Batch cultivation in shake flasks

One loopful of cells, propagated on YPD agar for 24 h at 30 °C, was used to inoculate the first preculture (25 mL YPD medium in 250 mL baffled flasks), which was incubated on a rotary shaker (28 °C, 230 rpm, 75% humidity, Multitron, Infors AG, Bottmingen, Switzerland). After 8 h, cells were harvested (3000×*g*, 2 min, 20 °C), inoculated into the second preculture (50 mL YPD medium in 500 mL baffled flasks) at an initial $OD_{600} = 0.1$, and grown overnight under the same conditions. Then, cells were harvested as described above and used to inoculate the main cultures at an initial $OD_{600} = 1$ (50 mL YPD medium in 500 mL baffled flasks) and grown under the same conditions. All experiments were conducted in biological triplicate.

2.4. Benchmarking of DHA production in lab-scale bioreactors

The performance of DHA production was evaluated in 1 L lab-scale bioreactors which were monitored and controlled using DASGIP control software (SR0700ODLS, Eppendorf, Hamburg, Germany). Six different process configurations were tested, including three batch and three fed-batch setups. Therefore, different media (500 mL) were used. First, (reference) 100 g of glycerol, 5 g of $(NH_4)_2SO_4$, 1.04 g of MgSO4 · 7 H2O, 1 g of KH_2PO_4, 130 mg of $CaCl_2 \cdot 2\,H_2O$, 100 mg of NaCl, 33 mg of $FeCl_3 \cdot 6\,H_2O$, 5 mL of a vitamin solution (200 mg L^{-1} inositol, 40 mg L^{-1} calcium pantothenate, 40 mg L^{-1} nicotinic acid, 40 mg L^{-1} pyridoxine · HCl, 39 mg L^{-1} thiamine · HCl, 20 mg L^{-1} aminobenzoic acid, 20 mg L^{-1} riboflavin, 0.2 mg L^{-1} biotin, 0.2 mg L^{-1} folic acid), 5 mL of a trace element solution (71 mg L^{-1} $ZnSO_4 \cdot 7\,H_2O$, 50 mg L^{-1} boric acid, 45 mg L^{-1} $MnSO_4 \cdot H_2O$, 23.5 mg L^{-1} $Na_2MoO_4 \cdot 2\,H_2O$, 10 mg L^{-1} NaCl, 4 mg L^{-1} $CuSO_4$, pH = 1.0) and 200 mM MES buffer (pH 6.5) were used. Second (phosphate-enriched), 100 g of glycerol, 5 g of $(NH_4)_2SO_4$, 2 g of KH_2PO_4, 1.04 g of MgSO4 · 7 H_2O, 130 mg of $CaCl_2 \cdot 2\,H_2O$, 100 mg of NaCl, 33 mg of $FeCl_3 \cdot 6\,H_2O$, 5 mL of vitamin stock, 5 mL of trace element stock, and 200 mM MES (pH 6.5) were added per liter. Third (nitrogen-enriched), 100 g of glycerol, 10 g of $(NH_4)_2SO_4$, 1.04 g of MgSO4 · 7 H2O, 1 g of KH_2PO_4, 130 mg of $CaCl_2 \cdot 2\,H_2O$, 100 mg of NaCl, 33 mg of $FeCl_3 \cdot 6\,H_2O$, 5 mL of vitamin stock, 5 mL of trace

element stock, and 200 mM MES (pH 6.5) were added per liter. The three media were additionally used for the batch phase of three fed-batch processes, which additionally included the pulse-wise feeding of L-lysine from a concentrated stock (3.0 M), resulting in a total of six different conditions. During the process, antifoam 204 (Sigma Aldrich) was added manually when needed.

In all cases, one loopful of cells, propagated on YPD agar for 24 h at 30 °C, was used to inoculate the first preculture (3 × 50 mL YPD medium in 500 mL baffled flasks), which was incubated on a rotary shaker (28 °C, 230 rpm, 75% humidity, Multitron, Infors AG, Bottmingen, Switzerland). After 8 h, cells were harvested (3000×*g*, 2 min, 20 °C), inoculated into the second preculture (3 × 100 mL YPD medium in 1000 mL baffled flasks) to an initial $OD_{600} = 0.1$, and grown overnight under the same conditions. Then, cells were harvested as described above and used to inoculate cultures for the production process. During the process, the temperature was kept at 28 °C ± 0.1 (CWD4 Bioblock, Eppendorf). The pH value was controlled above 3.0 ± 0.1 using a pH probe (405-DPAS–SC–K8S/225, Mettler Toledo, Giessen, Germany) and automatic addition of 6 M NaOH (MP8 pump system, Eppendorf). The level of dissolved oxygen (DO) was monitored using an electrode (Hamilton, Höchst, Germany) and controlled (above 20% saturation during the initial growth phase and above 5% saturation afterward) by automatic adjustment of stirrer speed (up to 1500 rpm) and aeration rate (up to 1 VVM). Experiments in every condition were performed in duplicate.

2.5. Quantification of cell concentration

The cell concentration was inferred from photometric measurement of the optical density at a wavelength of 600 nm (OD_{600}). In addition, the cell dry mass (CDM) was determined gravimetrically after cell harvest (15,000×*g*, 4 °C, 10 min), washing of the obtained pellet with 15 mL deionized water, and freeze drying. Systematic parallel measurements provided a linear correlation between CDM and OD_{600} (CDM [g L^{-1}] = 0.424 × OD_{600}), which enabled us to infer the CDM values from OD_{600} readings.

2.6. Quantification of glucose, glycerol, citrate, and acetate

The supernatant was obtained from the broth by centrifugation (16,000×*g*, 3 min, 4 °C). Glucose, glycerol, citrate, and acetate were then quantified by HPLC (Agilent 1200 series, Waldbronn, Germany) using an Aminex HPX-87H column (300 × 7.8 mm, 9 μm, Bio-Rad, Hercules, CA, USA) at 45 °C and elution with 12 mM H_2SO_4 at a flow rate of 0.5 mL min^{-1}. The analytes were detected by refraction index, and external standards were used for quantification.

2.7. Quantification of phosphate and ammonium

Phosphate and ammonium were quantified by ion exchange chromatography (Dionex Integrion HPIC System, Thermo Fisher Scientific, Waltham, MA, USA). Phosphate was quantified using a Dionex IonPac AS9-HC column at 30 °C (2 × 250 mm, Thermo Fisher Scientific) as the stationary phase and 12 mM Na_2CO_3 (0.25 mL min^{-1}) as the mobile phase. Ammonium was quantified using a Dionex IonPac CS column at 40 °C (2 × 250 mm, Thermo Scientific, CA, USA) as the stationary phase and 30 mM methanesulfonic acid (0.16 mL min^{-1}) as the mobile phase. Both ions were detected using suppressed conductivity analysis and quantified *via* external standards.

2.8. Quantification of fatty acids

A culture volume containing approximately 5 mg of CDM was sampled, centrifuged (12,000×g, 5 min, 4 °C), and dried (Savant DNA120 SpeedVac Concentrator, Thermo Scientific, 60 min, 65 °C). Then, 15 μg of the methyl ester of n-3 heneicosapentaenoic acid (HPA, C22:5) (Cayman Chemical, Ann Arbor, MI, USA) was added as an internal standard. Subsequently, transesterification of the fatty acids into the corresponding fatty acid methyl esters (FAMEs) was carried out by adding 300 μL of reagent (50% methanol, 50% toluene, 2% H_2SO_4) and incubating the mixture overnight at 80 °C. Afterward, 250 μL of a stop solution (0.5 M NH_4HCO_3, 2 M KCl) was added, and the mixture was vortexed for 30 s followed by centrifugation (10,000×g, 5 min, room temperature). After phase separation, the upper phase containing the FAMEs was used for GC−MS analysis. The measurement was carried out on a gas chromatograph (Agilent 6890 N, Agilent Technologies, Santa Clara, CA, USA) equipped with an analytical capillary column (Agilent HP-88, 30 m × 250 μm × 0.2 μm, Agilent Technologies), and coupled to a mass-selective detector (5973 Network Mass Selective Detector, Agilent Technologies) (Sahin et al., 2018). Helium 5.0 was used as the carrier gas. Initially, the column temperature was kept at 110 °C for 1 min and was then increased by 4 °C min^{-1} up to 240 °C. This temperature was maintained for the rest of the measurement (33.5 min). For analysis, a 1 μL sample was injected at a split ratio of 5:1. Furthermore, the following temperature settings were used: inlet 250 °C, MSD transfer line 280 °C, ion source 230 °C, and quadrupole 150 °C.

2.9. Quantification of amino acids

Amino acids in the culture supernatant were quantified by HPLC (Agilent 1200 series, Agilent Technologies) after precolumn derivatization with *o*-phthaldialdehyde and fluorenylmethyloxycarbonyl chloride (Rohles et al., 2018a). The analytes were separated on a reversed-phase column (Gemini 5 μm C18 110 Å, 150 × 4.6 mm, Phenomenex, Aschaffenburg, Germany) at 40 °C using the following gradient of eluent A (20 mM NaH_2PO_4, 0.5 g L^{-1} sodium azide, pH 7.8) and B (45% acetonitrile, 45% methanol, 10% deionized water) at a flow rate of 1 mL min^{-1}: 0 min, 0% B; 0–44.5 min, 0–44.5% B; 44.5–45 min, 44.5–61.0% B; 45–48 min, 61–82% B; 48–48.5 min, 82–100% B; 48.5–51 min, 100-0% B. Fluorescence detection was carried out at 340/450 nm, and α-aminobutyric acid was used as an internal standard (Krömer et al., 2005).

2.10. Extraction and quantification of intracellular CoA-thioesters

Absolute quantification of CoA-thioesters was based on LC−ESI−MS/MS; the method was previously validated for different microbes, including *Y. lipolytica* (Gläser et al., 2020). To enable the accurate analysis of samples with high cell concentration and low abundance of the analytes of interest, the protocol was adapted as follows. Briefly, cells were collected (5 mg CDM during the exponential growth phase, 20 mg CDM during the stationary phase) and immediately mixed with 500 μL of a ^{13}C-labeled extract (prepared before from cells grown on 99% [$^{13}C_3$] glycerol, Cambridge Isotope Laboratories) and 5 mL ice-cold quenching solution (25 mM formic acid, 95% acetonitrile). The mixture was incubated for 10 min on ice. Cell debris was removed by centrifugation (15,000×*g*, 4 °C, 10 min), including two washing steps with 10 mL of supercold deionized water (Gläser et al., 2021). The supernatant was frozen in liquid nitrogen, freeze-dried, and resuspended in an acidic buffer (25 mM ammonium formate, 2% MeOH, pH 3.0, 4 °C). The CoA thioesters in the extract were analyzed using LC−ESI−MS/MS (QTRAP 6500+, AB Sciex, Darmstadt, Germany) coupled to an HPLC system (Agilent 1290 Infinity System, Agilent). The analytes were separated at 40 °C on a reversed-phase column (Kinetex XB-C18, 100 × 2.1 mm, 2.6 μ, 100 Å, Phenomenex, Aschaffenburg, Germany) using the following gradient of eluent A (50 mM formic acid, 25% ammonium hydroxide, pH 8.1) and eluent B (100% methanol) at a flow rate of 300 μL min^{-1}: 0–10% B (0–7 min); 10–100% B (7–10 min); 100% B (10–11 min); 100-0% B (11–12 min); 0% B (12–15). Multiple reaction monitoring (MRM) was used to detect acetyl-CoA, malonyl-CoA, succinyl-CoA, butyryl-CoA, hydroxybutyryl-CoA, 2-methyl-butyryl-CoA, crotonyl-CoA, propionyl-CoA, isovaleryl-CoA, and hydroxymethyl-glutaryl-CoA (HMG-CoA) (Gläser et al., 2020). Isovaleryl-CoA and

2-methyl-butyryl-CoA coeluted while exhibiting identical masses and were therefore analyzed as a lumped pool.

2.11. Extraction and quantification of intracellular amino acids

Intracellular amino acids were sampled and extracted using vacuum filtration (Wittmann et al., 2004). The protocol had been previously validated for different yeasts (Bolten and Wittmann, 2008). In brief, 0.5 mL of culture broth was filtered quickly through cellulose nitrate membranes (0.2 μm × 47 mm, Sartorius, Göttingen, Germany), including a washing step with deionized water. The cell-containing filter was transferred into boiling water (containing 220 μM α-aminobutyrate as an internal standard) and incubated at 100 °C for 15 min. The obtained extract was cooled on ice, clarified from debris (16,000×*g*, 4 °C, 5 min), and the amino acids were quantified by HPLC as described above.

2.12. RNA extraction

Cells were collected from 2 mL of broth (16,000×*g*, 4 °C, 30 s) and flash-frozen in liquid nitrogen. Total RNA was extracted and purified using the RiboPure RNA Purification Kit (Thermo Fisher Scientific). Purified RNA was then treated with the TURBO DNA-free Kit (Thermo Fisher Scientific) to remove remaining DNA, followed by RNA quantification (NanoDrop 1000 Spectrophotometer, Thermo Fisher Scientific) and quality control (RNA integrity number (RIN) > 8.5, RNA 6000 Nano kit, Agilent 2100 Bioanalyzer, Agilent Technologies).

2.13. Quantitative real-time PCR

Purified total RNA samples were subjected to another round of DNA digestion by the TURBO DNA-free Kit (Thermo Fisher Scientific). The resulting extracts were reverse-transcribed into cDNA (Maxima First Strand cDNA Synthesis Kit for RT−qPCR, Thermo Fisher Scientific). The obtained cDNA samples were then utilized for qPCR with the PowerUp SYBR Green qPCR Master Mix (Thermo Fisher Scientific) and selected primer pairs in a final volume of 20 μL (QuantStudio3, Thermo Fisher Scientific). The primers used were designed as 20 bp sequences of the target genes of interest (Supplementary file 1, Table S1). Their efficiency was validated in separate amplification reactions prior to application with different concentrations of primer and genomic DNA. All primers used in this study exhibited a proven efficiency between 0.9 and 1.2. The qRT−PCR cycles were conducted using the following parameters: hold stage (50 °C, 2 min; 95 °C, 2 min), 40 PCR cycles (95 °C, 15 s; 60 °C, 15 s; 72 °C, 1 min), and melt curve stage (96 °C, 15 s; 60 °C, 1 min; 95 °C, 15 s). The obtained data were processed by QuantStudio Design & Analysis Software (Thermo Fisher Scientific) using the built-in standard curve method. We used 26 S rDNA as an endogenous control for data normalization (Borkowska et al., 2020; Rodriguez et al., 2016; Theron et al., 2020) after validation (Supplementary file 1, Fig. S1). All samples were assessed *via* three biological replicates, and each sample was analyzed in three technical replicates.

2.14. Global gene expression profiling

Global gene expression profiling involved RNA reverse-transcription into cDNA, hybridization to a custom-made DNA microarray, and scanning (Kohlstedt et al., 2022). Briefly, the layout of the microarray was designed from target transcripts using the eArray online tool (Agilent). The created probes covered the entire genome of *Y. lipolytica* CLIB122 (assembly ASM252v1 CDS, GCA 000002525.1) (Dujon et al., 2004), which was functionally annotated using splicing site predictions and similarity searches *via* UniProtKB, BLAST and MycoCosm (Grigoriev et al., 2014); the integrated myxobacterial PUFA cluster genes encoding 17 enzymatic domains of the PKS complex (Gemperlein et al., 2019), were also utilized. The array covered all 7086 native genes of the yeast plus the genes of the heterologous PUFA cluster. For the latter, we designed 17 primers that were each specific to one of the 17 enzyme subunits of the PKS, encoded by the four genes *pfa1, pfa2, pfa3* and *ppt*. Three probes per target gene were designed in sense orientation with a length of 60 bp and a melting temperature (T_m) of 80 °C. Prior to analysis, 50 ng of pre-purified total RNA was clarified from the remaining DNA (TURBO DNA-free Kit, Thermo Fisher Scientific), reverse-transcribed into labeled cDNA and hybridized onto the microarray (One-Color Microarray-Based Exon Analysis – Low Input Quick Amp WT Labeling preparation protocol, Agilent Technologies). The hybridized slides were scanned (SureScan Microarray Scanner, Agilent Technologies), and the scans were processed (Feature Extraction Software, Agilent Technologies). The obtained raw data were analyzed with GeneSpring GX Software (Agilent Technologies). To minimize systematic nonbiological differences, the data were normalized using the percentile shift method. Statistical evaluation of the data was based on 3-way ANOVA. The fold change cutoff and the *P* value were set to 2 and ≤ 0.05, respectively. The 64 raw datasets obtained are accessible from the Gene Expression Omnibus (GEO) Database (GEO 224529). Each sample was analyzed in biological triplicate.

2.15. GC−MS for ^{13}C-labeling analysis of intracellular amino acids

The protocol for analysis of the ^{13}C labeling pattern of free intracellular amino acids was based on previous work with a related yeast (Schwechheimer et al., 2018a). In short, cells were sampled, and amino acids were extracted in boiling water, as described above. Then, the obtained extract was dried under nitrogen. For derivatization of the contained amino acids, 50 μL of N,N-dimethylformamide (1% pyridine) and 50 μL of MBDSTFA (N-(tert-butyldimethylsilyl)-N-methyltrifluoroacetamide, Macherey-Nagel, Düren, Germany) were added. The mixture was incubated for 35 min at 80 °C. Afterward, it was cooled down, clarified from debris (16,000×*g*, 5 min, 4 °C), and analyzed by GC−MS (GC 7890 A, MSD 5975C, Agilent Technologies) using an HP-5MS column (30 m, 250 μm × 0.25 μm, Agilent Technologies) with helium 5.0 as the carrier gas (1.7 mL min^{-1}). The ion clusters [M-57], [M-85], and [M-159], resulted from well-known fragmentation events by the imposed electron impact ionization (Schwechheimer et al., 2018b) and were successfully used before in ^{13}C experiments with other yeasts (Frick and Wittmann, 2005; Schwechheimer et al., 2018a). Initially, samples were analyzed in scan mode to exclude undesired isobaric matrix effects for the ion clusters to be used for labeling analysis (Wittmann, 2007). Afterward, the mass isotopomer distribution (MID) of validated amino acids of interest was assessed using selective ion monitoring (Supplementary file 1, Table S2). For validation, samples of naturally labeled *Y. lipolytica* cultures were analyzed to confirm that, in each case, the measured ^{13}C labelling pattern matched the theoretical value inferred from natural isotope abundance (Kohlstedt and Wittmann, 2019). The obtained MIDs were corrected for natural isotopes (van Winden et al., 2002).

2.16. LC−MS/MS for ^{13}C labeling analysis of intracellular CoA thioesters

Prior to ^{13}C analysis, 2 mL of cell broth was quenched in 10 mL ice-cold quenching solution (25 mM formic acid, 95% acetonitrile) and extracted. Then, the ^{13}C labeling pattern of selected CoA esters (acetyl-CoA, malonyl-CoA, succinyl-CoA) was assessed by LC−MS/MS analysis of ion clusters that allowed a clean quantification of the ^{13}C labeling in the contained acyl-residue using the MRM mode. Each CoA ester yielded a fragment at *m/z* 428 that corresponded to its adenosine-3,5-diphosphate-containing backbone but lacked the acyl group. The analysis of the mass isotopomer distribution of this ion cluster (*m*, 428; *m*+1, 429; *m*+2, 430; *m*+3, 431) provided information about the ^{13}C enrichment of the *de novo* synthetized backbone. This fragment was not enriched in ^{13}C for any of the CoA esters that were analyzed within 48 h after the ^{13}C tracer had been supplied. This revealed that the *de novo*

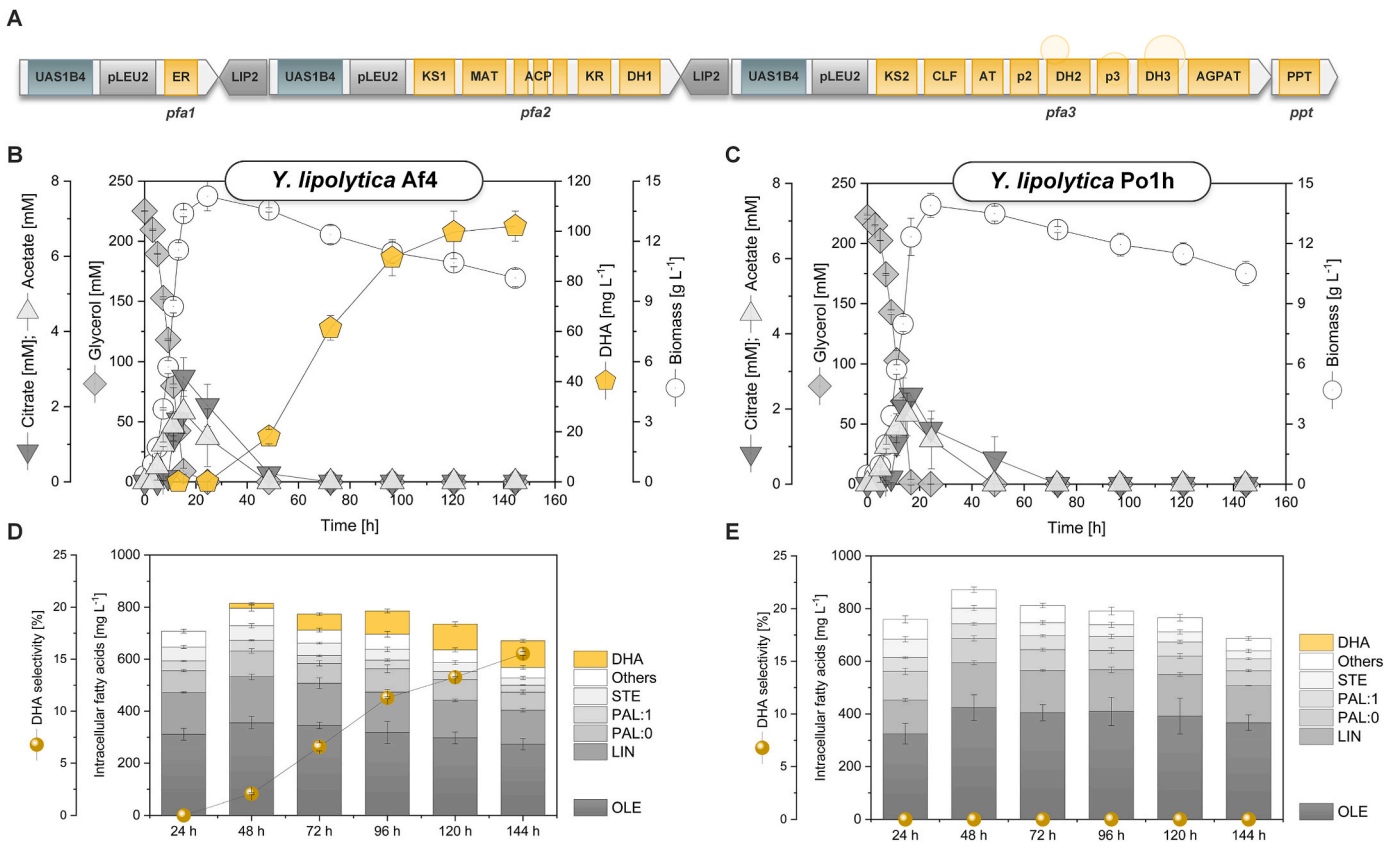

Fig. 1. Production of docosahexaenoic acid (DHA) in recombinant *Y. lipolytica* Af4 expressing a polyketide-synthase like complex-encoding gene cluster from the myxobacterium *A. fasciculatus*. The data show the structure of the heterologous gene cluster (A), and the cultivation profiles of the DHA-producing strain *Y. lipolytica* Af4 (B) and the parent wild-type (C) on minimal medium with 20 g L^{-1} (220 mM) of glycerol as the sole carbon source. The process exhibited three phases of exponential growth, early DHA production, and late DHA production, indicated in the plot by vertical dashed lines. In addition, the dynamic changes of the cellular content of native fatty acids and DHA during the process are revealed for the producer (D) and the wild type (E). These data were determined after extraction from biomass using GC/MS analysis of the corresponding FAME derivatives. PAL:0, palmitic acid (C16:0); PAL:1, palmitoleic acid (C16:1); STE, stearic acid (C18:0); OLE, oleic acid (C18:1); LIN, linoleic acid (C18:2); DHA, docosahexaenoic acid (C22:5). Other native fatty acids occurring in low amounts, such as docosanoic acid (C22:0), tetracosanoic acid (C24:0), and hexacosanoic acid (C26:0), are given as summed fractions. The data display means and standard errors from three biological replicates.

synthesis of the CoA ester backbone was insignificant during the time of the study. However, significant ^{13}C enrichment was detectable in the molecular ions $[M+H]^+$, which contained the (non-^{13}C-enriched) backbone plus the acyl residue. Therefore, analysis of the molecular ion allowed us to specifically infer the ^{13}C labeling pattern of the acyl group of each CoA ester. To this end, we analyzed the corresponding $[M+H]^+$ proton adducts (*m/z* 810–812 for acetyl-CoA, *m/z* 854–847 for malonyl-CoA, and *m/z* 868–872 for succinyl-CoA) using MRM. The outputs were corrected for natural isotopes (van Winden et al., 2002).

2.17. GC–MS for ^{13}C labeling analysis of fatty acids

FAMEs, extracted and derivatized as described above, were measured in scan mode (*m/z* 50–850) to evaluate signal quality and exclude isobaric overlay of the sample matrix with analyzed ion clusters (Wittmann, 2007). For native fatty acids (including C16:0, C18:0, C18:1, C18:2), the molecular ion (M^+) yielded a clean, prominent signal that matched the expected theoretical mass isotopomer distribution for nonenriched samples. This ion was therefore used to derive the corresponding MIDs. For DHA, the molecular ion was of too low quality and intensity to be used. Here, the *m/z* 313 ion fragment ($C_{21}H_{29}O_2$, formed upon loss of $–CH_3CH_2$ and containing carbons 3 to 22 of DHA) (Wang et al., 2019) was used for analysis after successful validation with non-labeled samples (Supplementary file 1, Fig. S2). Selected ion monitoring was performed in all cases to infer ^{13}C labeling patterns. All outputs were corrected for natural isotopes (van Winden et al., 2002).

2.18. Processing of ^{13}C labeling data

The output of the isotope correction (van Winden et al., 2002) represented the mass isotopomer fractions of an analyte's carbon skeleton (MID_{corr}). The outputs were used to derive total ^{13}C enrichment, termed summed fractional labeling (SFL) (Schwechheimer et al., 2018b), according to Eq. (1). The data are given in percent, whereby 100% represents a fully ^{13}C labeled carbon backbone, with *n* being the number of carbon atoms and *i* representing the number of ^{13}C atoms of an isotopomer.

$$SFL = \sum_{i=1}^{n+1} \frac{i * MID_{i,corr}}{n} * 100 \quad \text{(Eq. 1)}$$

3. Results and discussion

3.1. Yarrowia lipolytica Af4 exhibits stationary-phase production of DHA upon expression of a myxobacterial polyketide synthase-encoding gene cluster

Recently, the metabolically engineered strain *Y. lipolytica* Af4, expressing a biosynthetic gene cluster from the myxobacterium *Aetherobacter fasciculatus* (SBSr002) (Fig. 1A), was shown to overproduce DHA

(Gemperlein et al., 2019), a PUFA with multiple health benefits and recognized commercial value (Jovanovic et al., 2021). Here, we aimed to improve its production performance.

As a starting point to better understand the molecular processes that controlled (and eventually limited) the formation of DHA, we analyzed the growth and production dynamics of the engineered cell factory in glycerol-based cultures (Fig. 1B and D). The cells used up the carbon source (220 mM) within 24 h while accumulating a small amount of citrate (2.8 mM) and acetate (1.9 mM) as a result of metabolic overflow (Cavallo et al., 2017; Sabra et al., 2017). A biomass concentration of 14.3 g L^{-1} was reached at the end of the growth phase. The formed cells contained a substantial amount of native lipids, including saturated, mono- and di-unsaturated 18-carbon and 16-carbon fatty acids, mainly oleic acid (C18:1) and linoleic acid (C18:2), and, to a lower extent, stearic acid (C18:0) and palmitic acid (C16:0) overall revealing the typical profile of *Y. lipolytica* under these conditions (Carsanba et al., 2020) (Fig. 1D). In addition, traces of longer saturated fatty acids were present (C22:0, C24:0, C26:0), whereas the twenty-two carbon PUFA derivatives omega-3 and omega-6 docosapentanoic acid (DPA, C22.5), respectively, were not observed. DHA was not detectable during this initial process stage. The product started to visibly form only after 48 h, when glycerol had been consumed and cell growth had ended. During the following stationary phase, the DHA pool was constantly built up. At the end of the process, a final titer of 102 mg L^{-1} DHA was achieved. Obviously, the synthesis of DHA was decoupled from growth. The formation of PUFAs coincided with the re-consumption of extracellular citrate and the degradation of native lipids (Fig. 1B and D). In this regard, the PKS-driven strain exhibited a production mode that largely differed from previous strategies (Kujawska et al., 2021; Nazir et al., 2018), which, in fact, employed desaturases and elongases to derive PUFAs in *Y. lipolytica* during growth through artificially extended native fatty acid biosynthesis (Xue et al., 2013).

Compared to the producer, the wild type exhibited similar growth, glycerol consumption, and citric acid production (Fig. 1C) but a markedly different extent of lipid degradation during the stationary phase (Fig. 1E). On a quantitative basis, the wild type degraded 20% less native fatty acids (200 mg L^{-1}) than the engineered strain (250 mg L^{-1}) and, therefore, contained 17% more of them at the end of the process (687 mg L^{-1}) (Fig. 1E). When additionally considering DHA, which was exclusively synthetized in the producer, the level of total fatty acids, however, was almost the same in both strains. *Y. lipolytica,* due to its oleaginous nature, catabolizes intracellular lipid bodies during carbon starvation, suggesting that the newly formed DHA was, at least partially, synthesized from the native lipid pool through recycling processes (Liu et al., 2020; Shaigani et al., 2021).

The simultaneous breakdown of native fatty acids and the buildup of DHA in the producer enabled a continuous increase in product selectivity over time, so that DHA accounted for 17% of the total fatty acid pool (Fig. 1C). This seemed an advantage compared to growth-coupled production strategies, where the formation of DHA competes with native fatty acid biosynthesis and requires the use of expensive supplements such as cerulenin (Wan et al., 2016) and other biochemical stimulants (Hussain et al., 2021) to suppress the latter. When using glucose as a substrate instead of glycerol, the overall characteristics of growth and production were similar (Supplementary file 1, Fig. S3). Clearly, the growth-decoupled DHA production behavior was carbon source independent, even though the final DHA titer on glucose was 14.3% lower (Supplementary file 1, Table S3).

3.2. The onset of DHA production in Y. lipolytica Af4 coincides with reduced intracellular acetyl-CoA and malonyl-CoA levels

As shown, the production process exhibited the following three phases: (i) exponential growth on glycerol with native fatty acid, citrate, and acetate accumulation, (ii) early DHA production with parallel degradation of citrate, acetate, and native fatty acids, and (iii) late (weaker) DHA production with degradation of native fatty acids alone (Table 1).

For closer insight, we analyzed the intracellular pools of CoA esters that were linked to the metabolism of citrate and native fatty acids and to the formation of DHA, namely, acetyl-CoA, malonyl-CoA, and succinyl-CoA. During the initial growth phase, acetyl-CoA (650 nmol g^{-1}) was the most abundant CoA ester in *Y. lipolytica*, followed by succinyl-CoA (74 nmol g^{-1}) and malonyl-CoA (17 nmol g^{-1}) (Tables 2A and 2B). Remarkably, these CoA ester pools largely disappeared when the cells entered the stationary phase and started the production of DHA. The level of acetyl-CoA, the DHA starter unit, decreased by 96%.

Table 1
Dynamics of DHA production in recombinant *Y. lipolytica* Af4. The data display the specific rates related to the metabolism of citrate, acetate, DHA, and native fatty acids (FAs) during the three phases of glycerol-based batch cultures, highlighted in Fig. 1B. Positive values indicate formation, while negative values indicate consumption. The data display the average values and standard errors from three biological replicates. CDM, cell dry mass.

Exponential growth phase [mg g_{CDM}^{-1} d^{-1}]		Early DHA production phase [mg g_{CDM}^{-1} d^{-1}]		Late DHA production phase [mg g_{CDM}^{-1} d^{-1}]	
Citrate	124 ± 12	Citrate	−15 ± 4	Citrate	0 ± 0
Acetate	88 ± 7	Acetate	−6 ± 1	Acetate	0 ± 0
DHA	0 ± 0	DHA	2 ± 0	DHA	0.2 ± 0
Native FA	172 ± 8	Native FA	4 ± 1	Native FA	−8 ± 1

Table 2A
Dynamics of intracellular high-abundance CoA-thioesters during of docosahexaenoic acid (DHA) production in recombinant *Y. lipolytica* Af4. The samples were taken during the exponential phase (6 h, 10 h), the early stationary phase (24 h, 48 h) and the late stationary phase (72 h, 96 h) of the process (Fig. 1B). The absolute pool sizes were quantified using LC/MS-MS and ^{13}C-labeled internal standards (Gläser et al., 2020). The data display the average values and standard errors from three biological replicates.

[nmol g_{CDM}^{-1}]	6 h	10 h	24 h	48 h	72 h	96 h
Acetyl-CoA	685 ± 74	398 ± 83	47 ± 14	39.5 ± 13.9	39.4 ± 2.6	40 ± 6
Malonyl-CoA	17 ± 2	4 ± 1	0.3 ± 0.0	0.4 ± 0.1	0.2 ± 0.0	0.1 ± 0.0
Succinyl-CoA	78 ± 21	155 ± 66	34 ± 11	24 ± 13	39 ± 27	41 ± 21
Free-CoA	72 ± 7	138 ± 34	55 ± 12	36 ± 5	41 ± 6	52 ± 21

Table 2B
Dynamics of intracellular low-abundance CoA-thioesters during of docosahexaenoic acid (DHA) production in recombinant *Y. lipolytica* Af4. The samples were taken during the exponential phase (6 h, 10 h), the early stationary phase (24 h, 48 h) and the late stationary phase (72 h, 96 h) of the process (Fig. 1B). The absolute pool sizes were quantified using LC/MS-MS and ^{13}C-labeled internal standards (Gläser et al., 2020). The data display the average values and standard errors from three biological replicates.

[nmol g_{CDM}^{-1}]	6 h	10 h	24 h	48 h	72 h	96 h
Malonyl-CoA	16.5 ± 2.4	4.3 ± 1.3	0.3 ± 0.0	0.4 ± 0.1	0.2 ± 0.0	0.1 ± 0.0
Crotonyl-CoA	0.8 ± 0.1	1.7 ± 0.2	0.7 ± 0.1	0.6 ± 0.1	0.4 ± 0.0	0.3 ± 0.1
Butyryl-CoA	1.1 ± 0.1	3.4 ± 0.8	1.7 ± 0.3	1.3 ± 0.1	1.2 ± 0.3	0.9 ± 0.1
Propionyl-CoA	1.4 ± 0.2	1.9 ± 0.2	9.0 ± 1.7	4.3 ± 0.2	0.8 ± 0.0	0.7 ± 0.0
Isovaleryl-CoA	0.8 ± 0.3	1.5 ± 0.5	2.1 ± 0.4	2.7 ± 1.0	1.2 ± 0.8	0.7 ± 0.0
Hydroxy-methylglutaryl-CoA	11.0 ± 5.0	12.9 ± 2.1	26.7 ± 6.4	9.5 ± 3.2	4.4 ± 0.9	2.5 ± 0.2

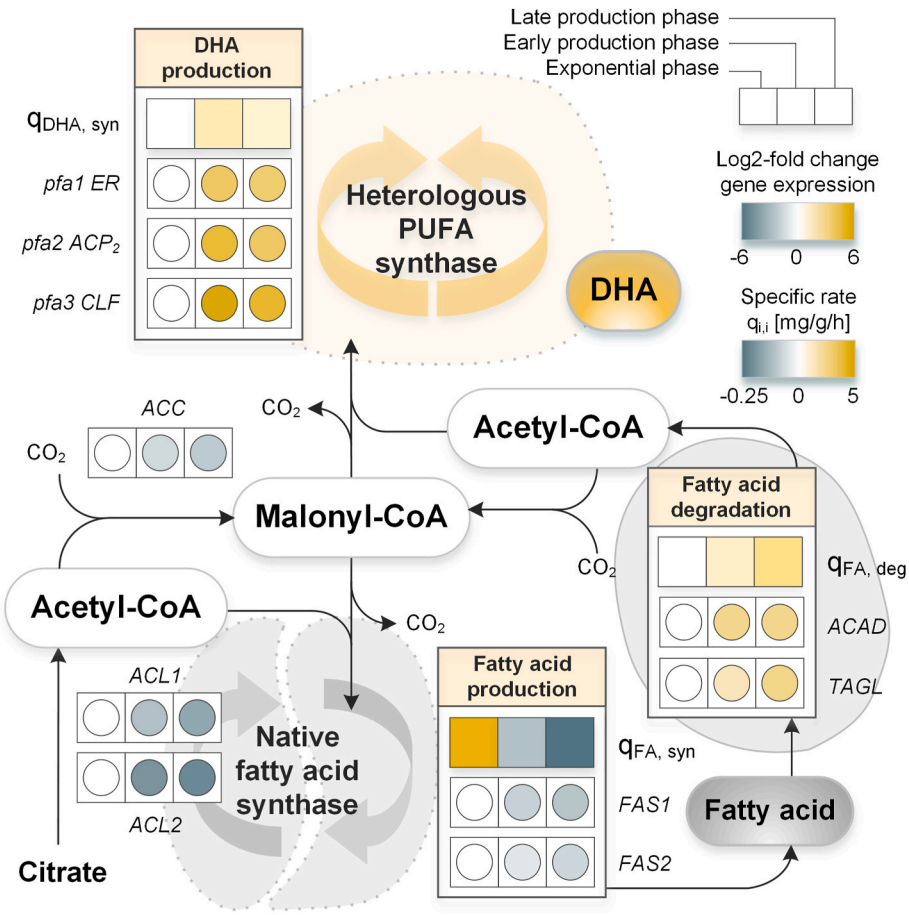

Fig. 2. Multi-omics profiling of DHA-producing *Y. lipolytica* Af4. The data include the levels of intracellular acetyl-CoA, malonyl-CoA, and succinyl CoA, assessed by LC–MS/MS using a ^{13}C labeled extract from cells grown on [$^{13}C_6$] glycerol for absolute quantification (Gläser et al., 2020). The concentrations were assessed at different time points during cultivation as follows: exponential growth phase (6 h, 10 h), early stationary phase (24 h, 48 h) and late stationary phase (72 h, 96 h) (Fig. 1B). In addition, the expression of selected genes was quantified using q-RT–PCR with the 26 S-RNA gene for normalization (Supplementary file 1, Fig. S1). The data refer to samples taken after 10 h, 48 h, and 96 h. In addition, the corresponding specific rates for DHA synthesis ($q_{DHA,syn}$), native fatty acid synthesis ($q_{FA,syn}$), and native fatty acid degradation ($q_{FA,deg}$) for each of the three process phases are displayed (Table 1). *ACL1, ACL2*, ATP-dependent citrate lyase (Beopoulos et al., 2012); *ACC*, acetyl-CoA carboxylase (Santin and Moncalian, 2018); *pfa1 ER*, enoyl reductase; *pfa2 ACP$_2$*, acyl carrier protein; *pfa3 CLF*, chain length factor, (Gemperlein et al., 2019). *FAS1, FAS2*, fatty acid synthase (Liu et al., 2019b); *ACAD*, acyl-CoA dehydrogenase (Haddouche et al., 2011; Mlickova et al., 2004); *TAGL*, triglyceride lipase (Dulermo and Nicaud, 2011).

Malonyl-CoA, of which 10 molecules are required to synthesize one DHA molecule, dropped by as much as 98% into the picomolar range (60 pmol g^{-1}). Sufficient precursor availability is known as a key requirement for metabolite overproduction (Lange et al., 2017; Rohles et al., 2018a, 2022), so the collapsing precursor levels at the onset of DHA production pointed to a potential bottleneck. Furthermore, the initially high abundance of the two CoA esters excluded the possibility that the absence of DHA formation during the exponential phase resulted from missing precursors.

In view of these changes, we studied relevant reactions around the supply and withdrawal of the two CoA esters at the level of transcription. For this purpose, we used q-RT–PCR with the 26 S rRNA gene for normalization (Supplementary file 1, Fig. S1). ATP citrate lyase was analyzed due to its significance in catalyzing the formation of cytosolic acetyl-CoA for fatty acid biosynthesis (Beopoulos et al., 2012). The expression of the two encoding genes *ACL1* and *ACL2* was high during the exponential growth phase but dropped 6-fold and 15-fold (log_2-fold changes of 2.6 and 3.9) with entry into the stationary phase, and the levels dropped even further towards the end of the process (Fig. 2). *Aspergillus niger* mutants that lack citrate lyase exhibit a significant decrease in acetyl-CoA (Chen et al., 2014), suggesting that the reduced expression of *ACL1* and *ACL2* contributed to the low abundance of this metabolite during the stationary phase, even though citrate was available for up to 48 h (Fig. 1C). The expression levels of *TAGL*, encoding triglyceride lipase, and *ACAD*, encoding acyl-CoA dehydrogenase, increased (log_2-fold increase of 1.7 and 2.5) when the cells entered the stationary phase. Both enzymes are involved in lipid degradation. At the same time, the expression of the native fatty acid synthase, which is responsible for *de novo* lipogenesis and encoded by *FAS1* and *FAS2* (Liu et al., 2019b), was downregulated.

The strongly increased expression of *pfa1*, *pfa2*, and *pfa3* revealed upregulation of the PKS cluster during the stationary phase. In contrast, *ACC*, encoding acetyl-CoA carboxylase, which is the exclusive source for cytosolic malonyl CoA (Santin and Moncalian, 2018), was found to be downregulated, likely contributing to the limited abundance of the precursor during later phases of the cultivation process (Table 2B). In this regard, the production of DHA was embedded into complex metabolic and transcriptional dynamics linked to cellular adaptation upon the shift from the growth to the stationary phase. Notably, metabolomic and transcriptomic analyses revealed a temporal mismatch between the expression of the heterologous pathway (stationary phase) and sufficient availability of the primer and chain extender DHA-precursors acetyl-CoA and malonyl-CoA (exponential phase).

3.3. *The overexpressed heterologous PKS-synthase complex faces a fundamental change in metabolism upon the shift from intracellular lipid synthesis to lipid degradation*

For a wider inspection of the cellular dynamics, we conducted a time series of global transcriptome analyses. The analysis, based on a custom-made microarray, provided a high level of agreement with q-RT–PCR results in terms of temporal expression behavior and the magnitude of changes, underlining the consistency of both methods (Supplementary file 1, Fig. S4). PCA of 24 wild-type and overproducer transcriptome datasets from different cultivation time points revealed generally high reproducibility between biological replicates (Supplementary file 1, Figs. S5 and S6). In addition, the PCA data revealed fundamental changes in global gene expression over time. Both strains revealed a continuous shift of the transcriptome that resulted in a different expression pattern in each of the three process stages. Differences in expression were hereby observed for key genes involved in DHA biosynthesis, citrate, and fatty acid metabolism, so we kept the division

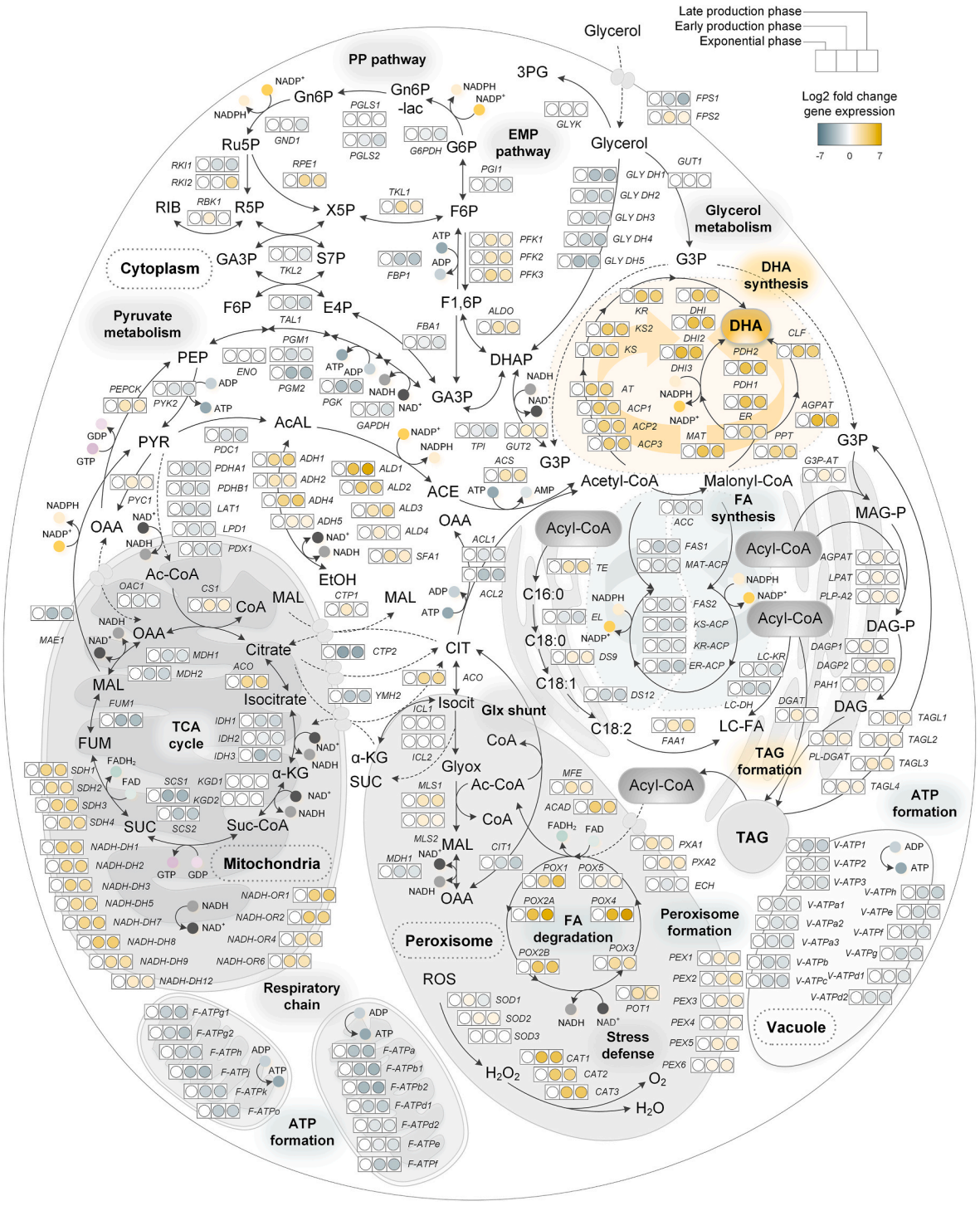

(caption on next page)

of the process into three phases in the following evaluation of experiments (Supplementary file 1, Fig. S4). Interestingly, the wild-type and overproducer strains exhibited a high concordance in global gene expression during exponential growth and early DHA production (Supplementary file 1, Figs. S5 and S6). Toward the end of the process, the global gene expression of the two strains drifted further apart, suggesting a stronger impact of the heterologous pathway during this phase (Supplementary file 1, Fig. S6, Supplementary file 1, Table S4). In numbers, the recombinant DHA producer changed the expression of 5323 genes (82% of its genetic repertoire) upon the shift from growth to early DHA production as follows: 3286 genes were up-regulated, and 2037 genes were downregulated. In comparison, 2118 genes were upregulated, and 3205 genes were downregulated in the late DHA production phase compared to the growth phase. As shown, cells were metabolically active during the entire culture period of 150 h, far longer than the average half-life of proteins (between less than one to a few hours) (Belle et al., 2006; Martin-Perez and Villén, 2017) and transcripts (in the range of a few minutes) (Wang et al., 2002) in related yeasts,

Fig. 3. Transcriptional dynamics within the carbon metabolism of *Y. lipolytica* Af4 expressing a myxobacterial PKS-like synthase for production of DHA from glycerol. The data reflect the gene expression at three different time points during the process, representing the exponential growth phase (10 h), the early stationary phase (48 h), and the late stationary phase (96 h) (Fig. 1B). They display average values from three biological replicates, normalized to expression at 10 h for comparison. The complete raw and processed datasets are available at the Gene Expression Omnibus Database (GEO 224529). The presented (approximately 200) genes encode the core metabolic machinery of the yeast, including glycerol utilization, citrate and acetate metabolism, the Emden-Meyerhof-Parnas (EMP) pathway, the pentose phosphate (PP) pathway, the TCA cycle, the glyoxylate shunt, CoA ester metabolism, intercompartmental transport, lipid synthesis, lipid breakdown, DHA formation, and stress defense. The genes encode glycerol uptake *via* aquaglyceroporin, *FPS1*, *FPS2 GLYDH*, glycerol dehydrogenase, *GUT1*, glycerol kinase, *GUT2*, G3P dehydrogenase (Erian et al., 2022; Lubuta et al., 2019); the PP pathway (Wasylenko et al., 2015; Yuzbasheva et al., 2017); the EMP pathway (Bian et al., 2018); *ADH*, alcohol dehydrogenase, *ALD*, aldehyde dehydrogenase (Liu et al., 2019a); the pyruvate dehydrogenase complex (*PDHA1, PDHB1, LAT1, LPD1, PDX1*) (Guo et al., 2014); *ACS*, acetyl-CoA synthetase (Gatter et al., 2016); the mitochondrial TCA cycle (da Silva et al., 2020); the peroxisomal glyoxylate shunt (Liu et al., 2016, 2019a); transporters for intercompartmental metabolite exchange, i.e., *OAC* (transport of oxaloacetate) (Luevano et al., 2010), *CTP1* (citrate/malate exchange), *CTP2* (transport of citrate), *YMH2* (citrate/α-ketoglutarate exchange) (Yuzbasheva et al., 2019), *PXA1*, PXA2, (transport of acyl-CoA) (Dulermo et al., 2015); *ACL1*, *ACL2*, ATP-dependent citrate lyase (Beopoulos et al., 2012); *ACC*, cytosolic acetyl-CoA carboxylase (Santin and Moncalian, 2018); *FAS1*, *FAS2*, fatty acid synthase (Liu et al., 2019b); *ACP*, acyl carrier protein, *TE*, thioesterase, *EL*, elongase, *DS9*, desaturase, DS12, desaturase, FAA1, long-chain fatty acid synthase (Wang et al., 2022); *AGPAT*, 1-acylglycerol-3-phosphate O-acyltransferase, *DAGP*, diacylglycerol diphosphate phosphatase, *DGAT*, acyl-CoA: diacylglycerol acyltransferase (Qiao et al., 2015), *TAGL1-4*, triglyceride lipase isoenzymes (Dulermo and Nicaud, 2011); *ACAD*, acyl-CoA dehydrogenase, *POX1*-6, peroxisomal acyl-CoA oxidase, *MFE*, multifunctional β-oxidation enzyme, *POT1*, ketoacyl thiolase (Haddouche et al., 2011; Mlickova et al., 2004); *PEX1-6*, assembly proteins for peroxisomal genesis and membrane formation (Kiel et al., 2006); *SOD1*-3, superoxide dismutase, *CAT*, catalase (Biriukova et al., 2006); V-ATP, vacuolar ATPases, F-ATP mitochondrial ATPases (Li et al., 2011), and *pfa1, pfa2, pfa3,* and *ppt*, polyketide synthase-like enzyme complex composed of 17 subdomains to synthesize DHA (Gemperlein et al., 2019). Abbreviations: G6P – glucose 6-phosphate, F6P – fructose 6-phosphate, F1,6 P – fructose 1,6-bisphosphate, GA3P – glyceraldehyde 3-phosphate, Gn6P – gluconate 6-phosphate, Ru5P – ribulose 5-phosphate, R5P – ribose 5-phosphate, RIB – ribose, X5P – xylulose 5-phosphate, S7P – sedoheptulose 7-phosphate, FUR6P – fructofuranose 6-phosphate, E4P – erythrose 4-phosphate, PEP – phosphoenolpyruvate, PYR – pyruvate, AcAL – acetaldehyde, ACE – acetate, OAA – oxaloacetate, α-KG – α-ketoglutarate, SUC – succinate, FUM – fumarate, MAL – malate, GLO – glyoxylate, 3 PG – 3-phosphoglycerate, DHAP – dihydroxyacetone phosphate, G3P – glycerol-3-phosphate, LC-FA – long-chain fatty acids, MAG-P – monoacylglycerol phosphate, DAG-P – diacylglycerol phosphate, DAG – diacylglycerol, TAG – triacylglycerol, ROS – reactive oxygen species.

suggesting on-going transcription and translation during the stationary phase under control of stationary phase promoters as observed in many microbes (Jaishankar and Srivastava, 2017). Various genes were changed in expression, illustrating that the transcriptional changes were global in nature (Supplementary file 1, Table S5). The affected genes included previously identified master regulators of a multi-scale network of lipid-associated gene that involves more than 100 transcription factors (Trebulle et al., 2017), regulators linked to the response to nitrogen limitation (Pomraning et al., 2016), as well as to morphological development (Pomraning et al., 2018) underlining the huge complexity of the changes. Given the relevance of the high-flux pathways of the central carbon metabolism for optimizing the overproduction of metabolites, experienced in our previous research (Hoffmann et al., 2021; Kind et al., 2014; Pauli et al., 2023; Weiland et al., 2023), we selected a subset of approximately 200 genes from these routes for further exploration (Fig. 3). These encoded proteins involved in glycerol, citrate and acetate metabolism, the Emden-Meyerhof-Parnas (EMP) pathway, the pentose phosphate (PP) pathway, the TCA cycle, the glyoxylate shunt, the pyruvate node, reactions linked to CoA ester metabolism, intercompartmental metabolite transport, lipid synthesis, lipid breakdown, DHA biosynthesis, ATP formation, redox metabolism, and stress defense.

Prominently, all four genes (*pfa1, pfa2, pfa3, ppt*) encoding the 17 subdomains of the myxobacterial PKS-like PUFA synthase (Gemperlein et al., 2014) were strongly upregulated, when cells entered the stationary phase, demonstrating that the delayed onset of DHA production was caused by a lack of transcription during the initial process. Genes encoding TAG lipases (*TAGL1*, *TAGL2*, *TAGL3*, *TAGL4*) and peroxisomal β-oxidation were found strongly upregulated, revealing the activation of lipid catabolism (Fig. 3). The expression ratio between the cytosolic ATP-dependent citrate lyase (*ACL1, ACL2*) and aconitase (*ACO*) in the cytosol and mitochondrion, respectively, shifted in favor of the latter (Holz et al., 2009), presumably promoting the conversion of citrate into isocitrate instead of oxaloacetate and acetyl-CoA. In terms of cytosolic acetyl-CoA supply, this adjustment competed with DHA production. The cytosolic isocitrate obviously entered the concomitantly activated peroxisomal glyoxylate shunt to fuel the conversion of acetyl-CoA from fatty acid degradation into four-carbon building blocks (Kamzolova et al., 2011; Lorenz and Fink, 2001). A contribution of the mitochondrial TCA cycle to citrate metabolization was indicated from the upregulation of the gene *CTP1*, encoding a mitochondrial citrate importer (Fig. 3). Genes encoding mitochondrial TCA cycle enzymes revealed a mixed expression response. While most of them were downregulated, succinate dehydrogenase (*SDH1, SDH2, SDH3, SDH4*) and citrate synthase (*CIT1*) were upregulated, together with the aforementioned mitochondrial aconitase. The succinate dehydrogenase complex has a unique dual function in that it couples the TCA cycle with the respiratory chain (Huang and Millar, 2013; Park et al., 1995). Notably, the complex has been identified as an important site for the generation of reactive oxygen species (Guzzo et al., 2014). The efficient elimination of oxidative stress is, however, regarded as major feature for successful overproduction of PUFAs to sustain cell viability and avoid peroxidation of the sensible reduced products (Jovanovic et al., 2021). The engineering of oxidative stress defense pathways in *Y. lipolytica* through the coupling of glutathione disulfide reductase and glucose 6-phosphate dehydrogenase along with aldehyde dehydrogenase were efficient solutions to combat reactive oxygen (Xu et al., 2017). Based on our data, it seems promising to evaluate succinate dehydrogenase as additional target towards increased oxidative stress tolerance. On the other hand, strain Af4 exhibited a strong upregulation of the oxidative stress defense system, including genes encoding superoxide dismutase and catalase isoenzymes (Fig. 3), beneficial to protect the sensitive DHA molecule from oxidation (Xu et al., 2017).

Cytosolic acetyl-CoA synthetase (*ACS*) was also upregulated, eventually linked to the reuse of acetate from the growth medium (Fig. 1C). Expression of the dihydroxyacetone-based pathway, the main route to catabolize external glycerol (Bellou et al., 2014), was downregulated, consistent with the fact that glycerol was already consumed at that time (Egermeier et al., 2017; Erian et al., 2022). The alternative G3P-based pathway was upregulated, likely to recycle G3P formed during TAG degradation back to DHAP and further upstream to glucose 6-posphate (Beopoulos et al., 2008; Dulermo and Nicaud, 2011). This upregulation of gluconeogenesis appeared beneficial for DHA production, which relies on the activity of the PP pathway to provide redox power for synthesis of the unsaturated fatty acid (Wasylenko et al., 2015).

In summary, the reduced intracellular level of acetyl-CoA during the stationary phase (Table 2A) demonstrated that the intermediate (continuously formed from degraded lipids) was strongly used up by other pathways. The complex transcriptional changes did not allow to assign the exact use of acetyl-CoA to specific pathways, but as the CoA ester was the major catabolic intermediate at this point, a broad distribution within the metabolic network appeared likely. At this point, the

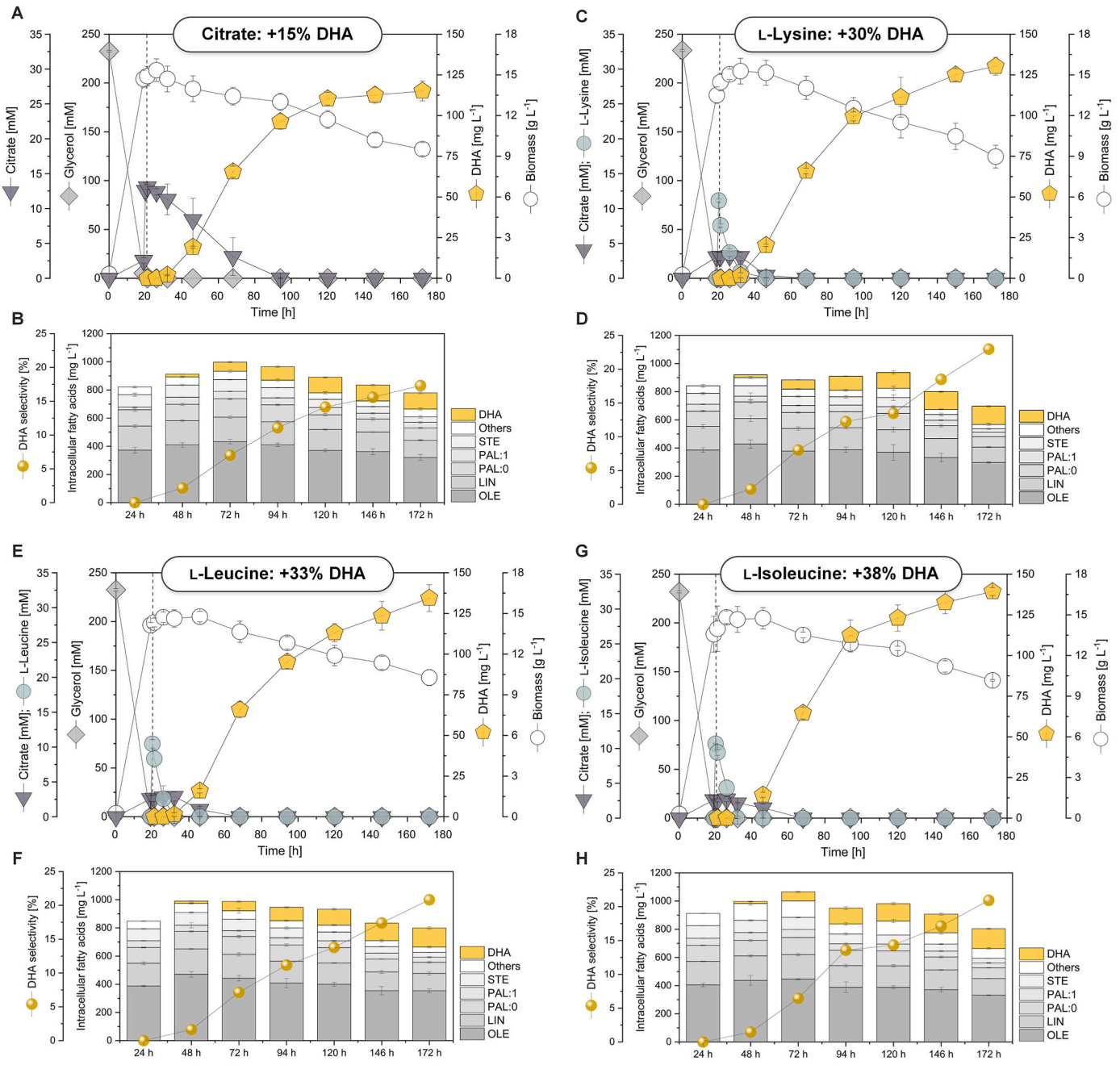

Fig. 4. Enhanced DHA production in recombinant *Y. lipolytica* Af4 upon supplementation with citrate (A, B), L-lysine (C, D), L-leucine (E, F), and L-isoleucine (G, H). The different supplements (10 mM each) were added at the end of the growth phase, when glycerol (220 mM) was depleted. The data represent the corresponding cultivation profiles (A, C, E, G) and changes in the cellular content of native fatty acids and DHA (B, D, F, H). The fatty acid content was determined after extraction from biomass using GC/MS analysis of the corresponding FAME derivatives. The process exhibited three phases of exponential growth, early DHA production, and late DHA production, as indicated by the vertical dashed lines. PAL:0, palmitic acid (C16:0); PAL:1, palmitoleic acid (C16:1); STE, stearic acid (C18:0); OLE, oleic acid (C18:1); LIN, linoleic acid (C18:2); DHA, docosahexaenoic acid (C22:6). Other native fatty acids occurring in low amounts, such as docosanoic acid (C22:0), tetracosanoic acid (C24:0), and hexacosanoic acid (C26:0), are given as summed fractions. The data display means and standard errors from three biological replicates.

shortage of acetyl-CoA and malonyl-CoA displayed a severe bottleneck at the level of precursor availability that was caused by the competition between DHA biosynthesis and central metabolism, deserving further exploration.

3.4. Spiked ^{13}C-citrate is catabolized via the TCA cycle and increases the pools of acetyl-CoA and malonyl-CoA for enhanced fatty acid synthesis

Citrate plays an important role, based on its re-utilization during the DHA production that was observed here and before (Jia et al., 2022). To further clarify its metabolism, we spiked 10 mM citrate into the medium at the beginning of the stationary phase (20 h, increasing the broth level to 13 mM) (Fig. 4A). The pulse provided an extended phase of citrate excess. Upon feeding, citrate was present for up to 100 h, and the organic acid was depleted after 60 h in the control. It was interesting to note that citrate was consumed two times faster in the supplemented culture (2.8 mg g^{-1} h^{-1}) compared to the control (1.4 mg g^{-1} h^{-1}), and its consumption was eventually triggered by the increased availability.

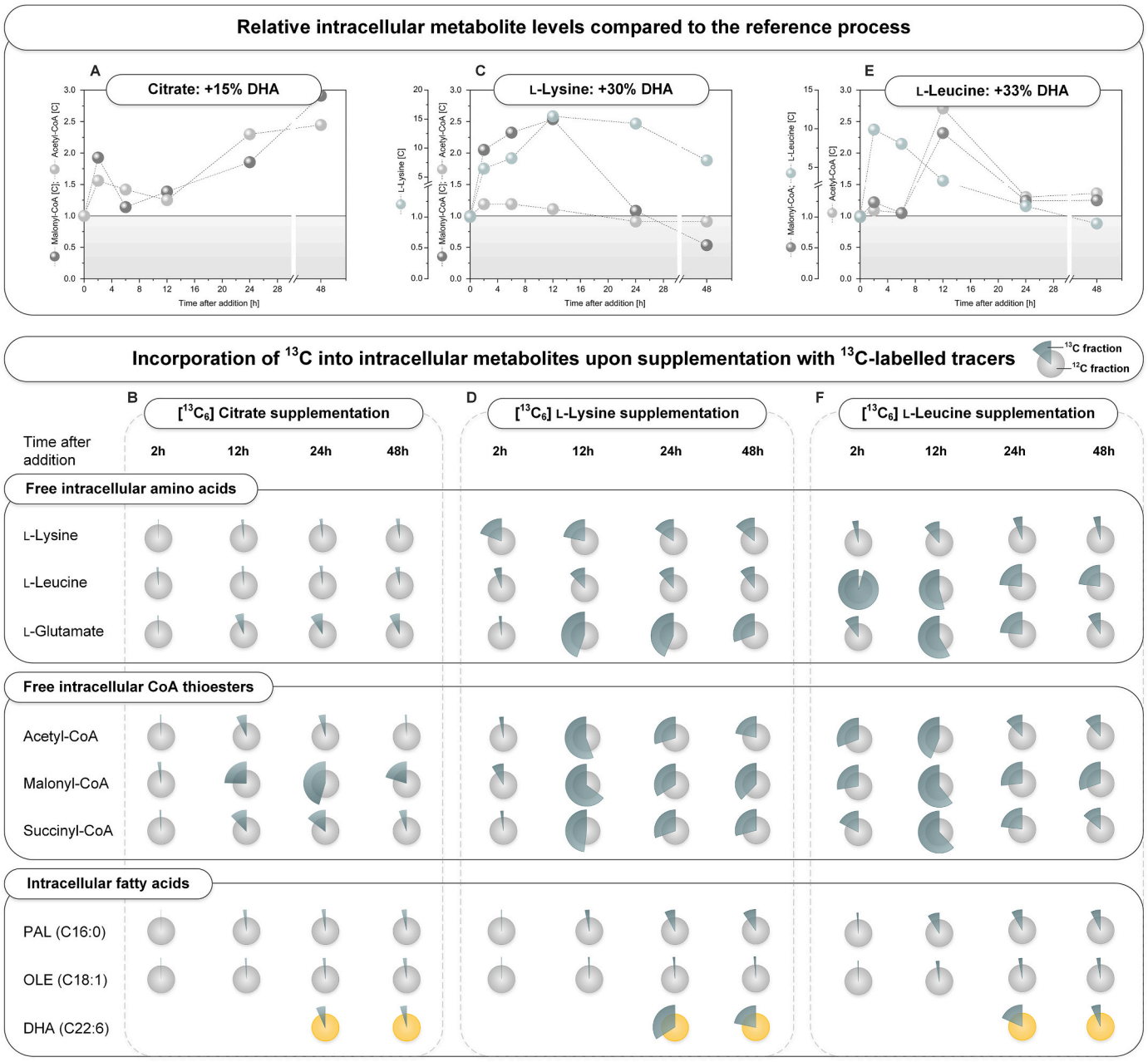

Fig. 5. Metabolic pathway profiling in DHA-producing *Y. lipolytica* using ^{13}C-labeled isotopic tracers. In separate experiments, 99% [$^{13}C_6$] citrate (A, B), 99% [$^{13}C_6$] L-lysine (C, D), and 99% [$^{13}C_6$] L-isoleucine (E, F) (each 10 mM) were spiked into the cultures at the end of the growth phase, when glycerol was depleted. This time point is given as 0 h here. The data comprise the dynamics of the intracellular pools of selected amino acids and CoA esters (A, C, E) after the addition of the corresponding tracer. The concentrations are given as relative values compared to the non-supplemented process. In addition, the data show dynamic changes in the ^{13}C enrichment of intracellular amino acids, CoA-esters, native fatty acids, and DHA, assessed by LC–MS/MS and GC/MS, 2 h, 12 h, 24 h, and 48 h after addition of the ^{13}C-based tracer. The data display means and standard errors from three biological replicates.

Favorably, citrate supplementation increased the synthesis of DHA. The relative fraction of DHA among total fatty acids (17%) was, however, unchanged due to a simultaneously stimulated synthesis of native fatty acids (Supplementary file 1, Table S6). The relative improvement of the DHA titer (15%) was slightly higher than the extra amount of supplemented carbon (10%), indicating a preference of citrate for DHA synthesis over other processes. Strikingly, the addition of citrate impacted the levels of intracellular CoA esters. It resulted in increased levels of acetyl-CoA and malonyl-CoA (Fig. 5A). Furthermore, the pool of succinyl-CoA was approximately doubled (Supplementary file 1, Fig. S7A), indicating that citrate was directed into the TCA cycle in the mitochondrion, the only pathway that can form succinyl-CoA in *Y. lipolytica* (Cui et al., 2017). Furthermore, the 40 h longer period of citrate excess provided an extra benefit in the later phases of culture. Two days after supplementation (when extracellular citrate was only left in the spiked culture), the abundance of acetyl-CoA and malonyl-CoA was still 2.3-fold and 2.9-fold higher, respectively.

In a separate experiment, we fed 10 mM 99% [$^{13}C_6$] citrate as an isotopic tracer after 20 h, which resulted in 13 mM 75% [$^{13}C_6$] citrate (3 mM of non-labeled citrate was present at this time point). We then monitored the ^{13}C enrichment in intracellular metabolites over time using GC/MS and LC–MS/MS. Notably, we detected prominent ^{13}C enrichment in CoA esters (Fig. 5B). As an example, malonyl-CoA exhibited 45% ^{13}C enrichment 24 h after the tracer had been added,

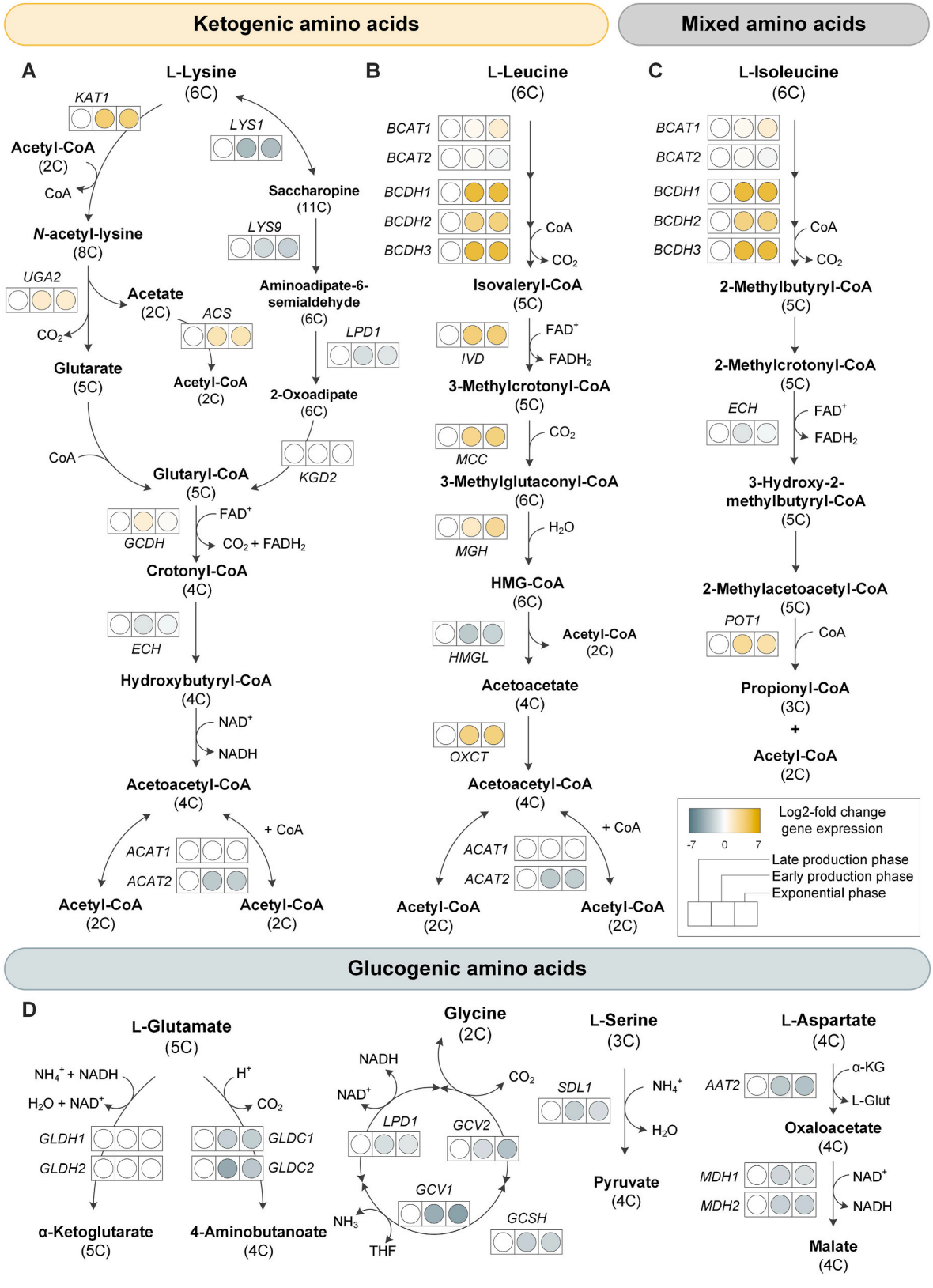

(caption on next page)

revealing that it originated to almost 60% from external citrate at this time point. The incorporation of ^{13}C labeling into succinyl-CoA proved that citrate was (at least partially) metabolized *via* the TCA cycle in the mitochondrion, matching the increase in succinyl-CoA abundance (Supplementary file 1, Fig. S7A) (Holz et al., 2011). Furthermore, free intracellular amino acids such as L-glutamate (10%), L-glutamine (13%),

Fig. 6. Transcriptional and metabolic dynamics around the amino acid and CoA-ester metabolism in DHA-producing recombinant *Y. lipolytica* Af4. The data comprise transcriptional changes in degradation pathways for the ketogenic amino acids L-lysine (A) and L-leucine (B), the mixed-type amino acid L-isoleucine (C), and the glucogenic amino acids L-glutamate, glycine, L-serine, and L-aspartate (D). The data refer to samples taken from a glycerol-based batch process after 10 h, 48 h, and 96 h and display means and standard errors from three biological replicates. *Y. lipolytica* uses L-lysine both as a nitrogen and as a carbon source *via* the *N*-6-acetyl-lysine-5 aminovalerate pathway (Barth and Gaillardin, 1997). Previously, the *LYC1* gene encoding the first step of the pathway, *N*-6-lysine acetyl transferase (LAT), was cloned and sequenced and shown to be induced by L-lysine (Beckerich et al., 1994). For completion, the additionally encoded saccharopine pathway is shown. The degradation of L-isoleucine and L-leucine is catalyzed by the same route, involving branched-chain amino acid aminotransferase (*BCAT1, BCAT2*), 2-oxoisovalerate dehydrogenase (*BCDH1, BCDH2*) and dihydrolipoyl transacylase (*BCDH3*) and several CoA-ester intermediates (Shao et al., 2018). Abbreviations: L-lysine-N-acetyltransferase (*KAT*), glutarate semialdehyde oxidoreductase (*UGA2*), acetyl-CoA synthetase (*ACS*), glutaryl-CoA dehydrogenase (*GCDH*), enoyl-CoA hydratase (*ECH*), acetyl-CoA acetyltransferase (*ACAT1*, *ACAT2*), branched chain amino acid aminotransferase (*BCAT1*, *BCAT2*), branched chain keto acid dehydrogenase (*BCDH*1, *BCDH2*, *BCDH3*), isovaleryl-CoA dehydrogenase (*IVD*), methyl-crotonyl-CoA carboxylase (*MCC*), methyl-glutaconyl-CoA hydratase (*MGH*), HMG-CoA lyase (*HMGL*), 3-oxoacid CoA-transferase (*OXCT*), 3-ketoacyl-CoA thiolase (*POT1*), L-glutamate:NADP dehydrogenase (*GLDH1, GLDH2*), L-glutamate decarboxylase (*GDC1, GDC2*), dihydrolipoamide dehydrogenase (*LPD1*), glycine decarboxylase (*GCV1, GCV2*), glycine cleavage system H protein (*GCSH*), L-serine dehydratase (*SDL1*), L-aspartate:2-oxoglutarate aminotransferase (*AAT2*), malate dehydrogenase (*MDH1, MDH2*).

and L-aspartate (11%) were significantly enriched in ^{13}C (Fig. 5B). These changes could not be attributed to a particular compartment due to the presence of isoenzymes of isocitrate dehydrogenase and L-glutamate dehydrogenase in the cytosol, mitochondrion, and peroxisome (Li et al., 2013; Pomraning et al., 2016). In fact, the occurrence of ^{13}C in all detected amino acids at later stages indicated a broad metabolic use of citrate (Supplementary file 1, Table S7). Strikingly, we proved the incorporation of citrate-derived carbon into native fatty acids such as PAL and OLE and into the heterologous product DHA (Fig. 5B). DHA ^{13}C labeling reached a maximum (7% after 24 h), indicating a transient shift from the use of citrate to the use of fatty acids related to the onset of lipid degradation and citrate depletion (Fig. 5B, Supplementary file 1, Fig. S8). Undoubtedly, the beneficial effects of supplementing citrate to increase precursor availability during DHA production appeared valuable to be optimized further.

3.5. *Y. lipolytica activates the catabolic breakdown of ketogenic and mixed-type amino acids upon starvationto replenish its intracellular CoA pools*

Acetyl-CoA is a precursor, intermediate, and product of many metabolic pathways (Vorapreeda et al., 2012). Interestingly, the metabolite is formed during the degradation of certain amino acids. The catabolization of the ketogenic amino acids L-lysine and L-leucine ultimately yields two or three molecules of acetyl-CoA, different from glucogenic amino acids which end up in other intermediates (Woolfson, 1983). L-isoleucine, for example, belongs to a third group and exhibits a mixed type, forming one acetyl-CoA among other intermediates (D'Andrea, 2000). Given the previous findings, it appeared straightforward to study these catabolic pathways in more detail.

Table 3
The impact of supplementation on docosahexanoic acid (DHA) production in recombinant *Y. lipolytica* Af4. Each supplement was added when the cells had depleted glycerol (Fig. 2). The given biomass concentrations are the maximum values, which were achieved at the end of the growth phase. The DHA titer and selectivity reflect the values at the process end, whereas the specific productivity represents the average over the entire process. The data display the average values and standard errors from three biological replicates. Statistical significance was based on a paired *t*-test. CDM, cell dry mass; TFA, total fatty acids.

Supplement [10 mM]	Biomass [g_{CDM} L^{-1}]	DHA titer [mg L^{-1}]	DHA selectivity [% of TFAs]	DHA productivity [mg L^{-1} d^{-1}]
–	10 ± 1	101 ± 7 [b]	17 ± 1	17 ± 2 [b]
Citrate	10 ± 0	115 ± 6 [a]	17 ± 0	19 ± 1 [a]
L-Lysine	9 ± 1	**130 ± 6** [a,b]	**23 ± 1** [a,b]	**21 ± 1** [a]
L-Leucine	10 ± 0	**134 ± 8** [a]	**20 ± 0** [a,b]	**21 ± 2**
L-Isoleucine	10 ± 0	**139 ± 3** [a,b]	**21 ± 0** [a,b]	**7 ± 1** [a,b]

[a] Significantly different from the reference.
[b] Significantly different from supplementation with citrate.

The transcriptome data of the DHA producer provided an interesting picture. When the cells entered the stationary phase at the onset of DHA production, they strongly upregulated genes encoding enzymes involved in the degradation of acetyl-CoA-delivering amino acids, i.e., L-lysine (log2-fold up to 4.3), L-leucine (log2-fold up to 5.5), and L-isoleucine (log2-fold up to 5.5) (Fig. 6A, B, and C, Supplementary file 1, Table S8). These changes indicated the activation of catabolic routes for ketogenic amino acids to replenish the acetyl-CoA pool during the stationary phase (Sabra et al., 2017). In contrast, degradation pathways for glucogenic amino acids (not yielding acetyl-CoA) were downregulated, especially those for L-glutamate, glycine, L-serine, and L-aspartate (log2-fold up to −4.3) (Fig. 6D, Supplementary file 1, Table S8).

The degradation of L-lysine, L-leucine, and L-isoleucine proceeds *via* HMG-CoA, isovaleryl-CoA, crotonyl-CoA, hydroxybutyryl-CoA, and propionyl-CoA, respectively (Park et al., 2020) (Fig. 6A, B, and C). As shown, *Y. lipolytica* contained a rich set of intracellular CoA esters with three to six carbon side chains in all growth stages (Table 2), in contrast to the rather limited short-chain CoA ester repertoire found in *S. cerevisiae* (Krink-Koutsoubelis et al., 2018).

Strikingly, the pools of HMG-CoA, isovaleryl-CoA, and propionyl-CoA, displaying intermediates from L-leucine and L-isoleucine catabolism, respectively, were increased more than fourfold in stationary-phase cells compared to exponentially growing cells (Table 2B). In accordance with the transcriptome data, this accumulation indicated enhanced degradation of these amino acids. Interestingly, the intracellular levels of free L-lysine, L-leucine, and L-isoleucine remained rather constant (Supplementary file 1, Table S9). Obviously, these pools were constantly fueled by degraded protein, matching the generally increased expression of genes encoding the protein degradation machinery (Supplementary file 1, Table S10). Taken together, these results show that the yeast utilized different internal resources, including lipid-derived fatty acids and protein-derived (mainly ketogenic) amino acids, to fuel its central carbon metabolism during the stationary phase. Acetyl-CoA was the central hub, where the activated catabolic pathways merged.

3.6. *Enhanced catabolization of L-lysine, L-leucine, and L-isoleucine boosts intracellular acetyl-CoA and malonyl-CoA availability and selective DHA production*

The obtained picture inspired us to explore individual amino acid feeding strategies. We therefore ran additional *Y. lipolytica* cultures that were supplied with 10 mM L-lysine, L-leucine, and L-isoleucine when glycerol was depleted (Fig. 4C, E, and G).

In all cases, the supplementation enabled a remarkable increase in DHA production (Fig. 4C, E, and G). The final DHA titer was increased by 30%, 33%, and even 38% when adding small amounts of L-lysine, L-leucine, and L-isoleucine, respectively (Table 3). Furthermore, the supplemented cultures achieved a far higher selectivity in production. As an

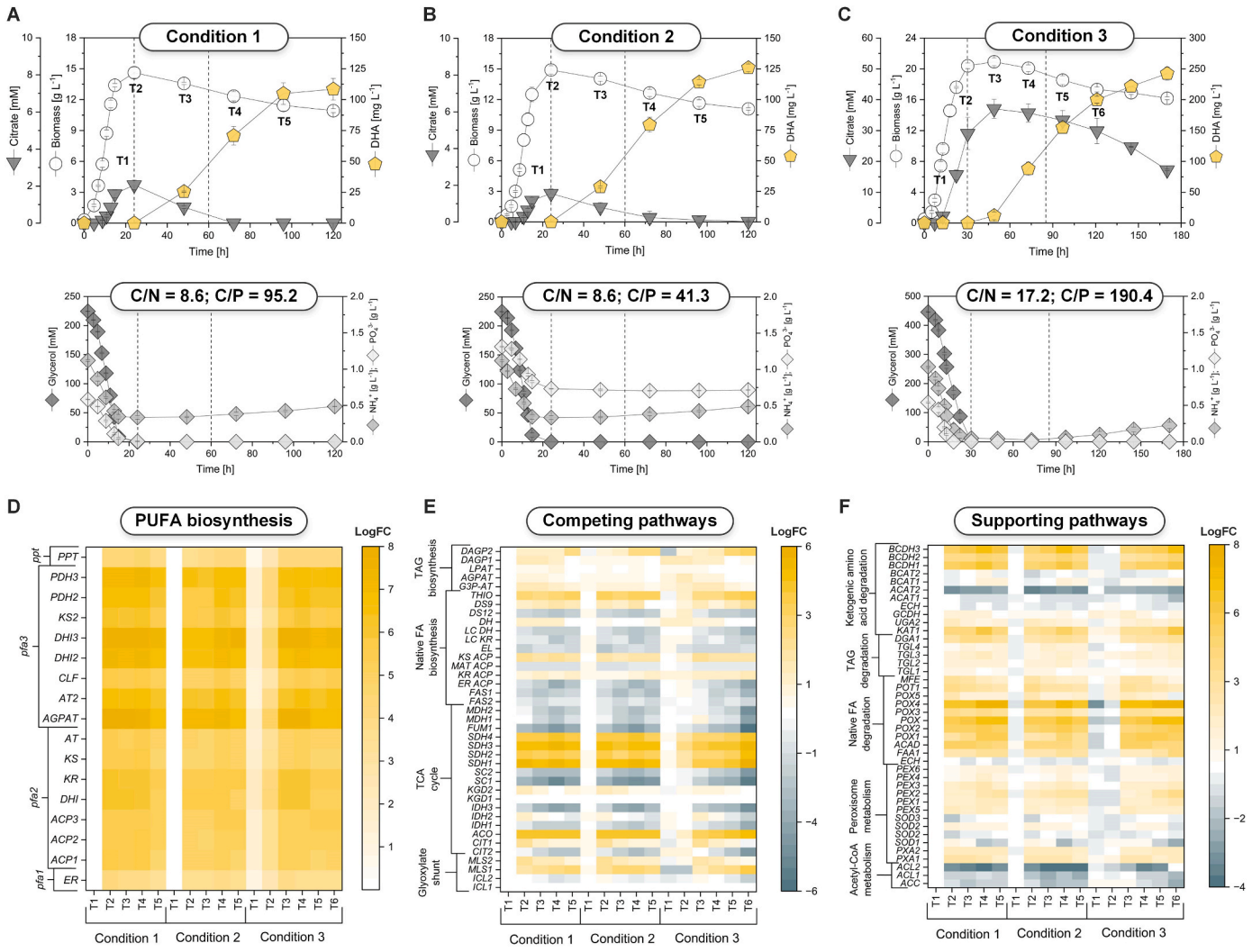

Fig. 7. Impact of the ratio of carbon, nitrogen, and phosphorous on the production of docosahexaenoic acid (DHA) in recombinant *Y. lipolytica* Af4. The data show the cultivation profiles from three set-ups using (i) minimal medium with 20 g L^{-1} (220 mM) of glycerol, 5 L^{-1} $(NH_4)_2SO_4$, 1 g L^{-1} of KH_2PO_4 (A), (ii) minimal medium with 20 g L^{-1} (220 mM) of glycerol, 5 L^{-1} of $(NH_4)_2SO_4$, 2 g L^{-1} of KH_2PO_4 (B), and (iii) minimal medium with 40 g L^{-1} (440 mM) of glycerol, 5 L^{-1} of $(NH_4)_2SO_4$, and 1 g L^{-1} of KH_2PO_4 (C). The processes are divided into three phases of exponential growth, early DHA production, and late DHA production, as indicated by the vertical dashed lines. Each of them was additionally studied at the transcriptome level at five time points (T1-T5) for the first two setups (A, B) and at six time points (T1-T6) for the third setup (C). All data were normalized to the gene expression levels of T1 in the reference process (A). They comprise the four genes *pfa1*, *pfa2*, *pfa3*, and *ppt*, encoding the 17 subdomains of the PKS-synthase complex for DHA synthesis (D), genes encoding competing pathways that withdraw CoA precursors, i.e. the glyoxylate shunt, the TCA cycle, the native fatty acid (FA) synthesis including elongation and desaturation, and tri-acyl-glycerol (TAG) synthesis (E). In addition, genes encoding supporting pathways that provide CoA thioesters for DHA synthesis, i. e. acetyl-CoA and malonyl CoA metabolism, ketogenic acid amino catabolism, peroxisome assembly and metabolism, as well as TAG and native FA degradation (F). All data display means and standard errors from three biological replicates. The complete raw and processed transcriptome datasets are available at the Gene Expression Omnibus Database (GEO 224529). A list of the encoded enzymes can be found in the supplement (Supplementary file 1, Table S11).

example, L-lysine feeding yielded an almost 40% higher content of DHA among total fatty acids (Fig. 4D, F, and H, Table 3), resulting from an increased degradation of native fatty acids in this process (Supplementary file 1, Table S6). In this regard, supplementation with ketogenic and mixed-type amino acids emerged as a smart way to boost heterologous PUFA synthesis in *Y. lipolytica*. In terms of production increase, each of the amino acids was two-to threefold more efficient than citrate and glycerol, resulting in only a 15% and 10% increase in DHA titer when adding the same amount of carbon, respectively. It was therefore interesting to study the underlying metabolic processes in more detail.

Upon addition, the amino acids were immediately consumed. Interestingly, they were each taken up at a similar rate: 4.0 mg g^{-1} h^{-1} for L-lysine, 3.5 mg g^{-1} h^{-1} for L-leucine and 3.6 mg g^{-1} h^{-1} for L-isoleucine. They were depleted from the medium within 12 h (Fig. 4C, E, and G). The production of DHA, however, was still enhanced more than 100 h later, which was surprising at first glance. However, amino acid supplements have been shown to trigger delayed metabolic effects in other microbes (Gläser et al., 2021). Indeed, the levels of intracellular CoA esters were significantly increased by supplementation, and these changes lasted a long time. We observed up to 2-fold higher levels of acetyl-CoA and malonyl-CoA (Fig. 5C and E). Furthermore, addition of the amino acids resulted in increased levels of succinyl-CoA (Supplementary file 1, Figs. S7B, C, and D). Interestingly, specific intermediates such as 3-hydroxy-3-methylglutaryl CoA (HMG-CoA), isovaleryl-CoA, crotonyl-CoA, and 2-methylbutyryl-CoA, respectively, resulting from the degradation of the added amino acids increased in concentration up to almost 200-fold (Supplementary file 1, Figs. S9D, E, and F). Notably, the CoA ester pools remained increased for a long time after the amino acid had been depleted. As an example, the pools of acetyl-CoA and malonyl-CoA were found to be twofold increased, even 36 h after

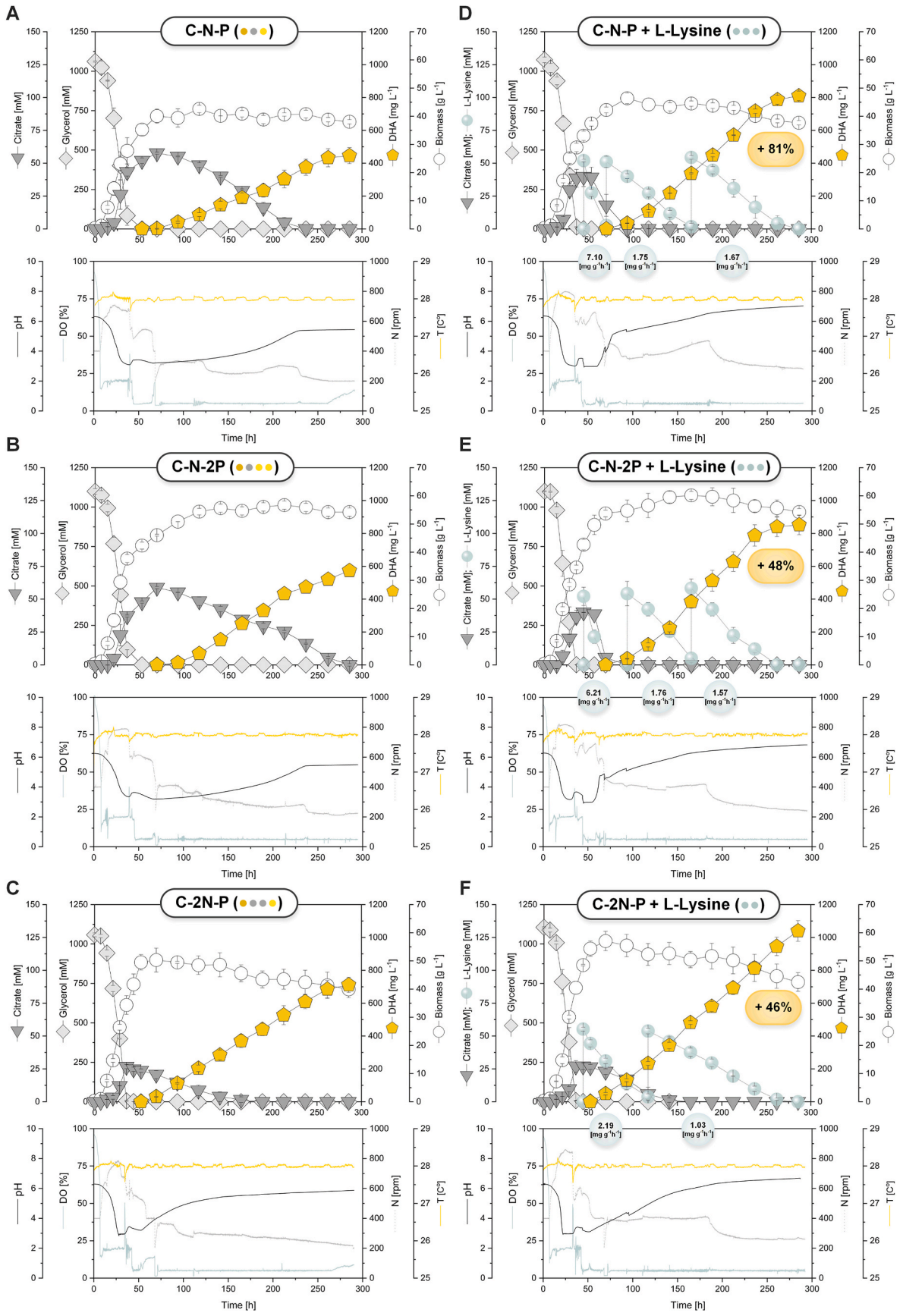

(caption on next page)

Fig. 8. Benchmarking the production of docosahexaenoic acid (DHA) in recombinant *Y. lipolytica* Af4 in lab scale bioreactors. The processes were based on different nutrient regimes (Table 4). The basic batch medium contained 100 g L^{-1} of glycerol, 5 g L^{-1} of $(NH_4)_2SO_4$, and 1 g L^{-1} of KH_2PO_4 as sources for carbon, nitrogen, and phosphorous (A). Additional setups comprised double amounts of nitrogen (C) and phosphorous (E). Each configuration was operated as a batch process. In addition, each set-up was additionally supplemented during the stationary phase with small shots of L-lysine during the DHA production phase (B, D, F). The data represent the cultivation profile and online monitored process parameters including the pH value, the dissolved oxygen (DO) level, the stirring rate (N) and the process temperature (T). In addition, the specific L-lysine uptake rate (mg g^{-1} h^{-1}), following each pulse, is provided. The data display means and deviations from two biological replicates.

L-isoleucine had been depleted (the last time point analyzed) (Supplementary file 1, Fig. S7D).

3.7. Isotopic ^{13}C tracer studies reveal substantial carbon flux from degraded ketogenic amino acids to replenish intracellular CoA esters and synthesize DHA

An interesting picture was observed for the pools of free intracellular L-lysine, L-leucine, and L-isoleucine. The changes in L-leucine and L-isoleucine were strong but lasted only a relatively short amount of time. Within a few hours, the corresponding intracellular level of the supplemented amino acid sharply rose in each of the two processes (up to tenfold). Afterward, it decreased and reached the level of non-supplemented cells within 12 h (L-isoleucine) and 24 h (L-leucine). In comparison, the intracellular pool of L-lysine was boosted the most upon supplementation (up to 15-fold), and the increased level was maintained for a longer time. Cells contained tenfold more L-lysine than non-supplemented cells, even 48 h after L-lysine had been added (Fig. 5). Notably, *Y. lipolytica* strains store L-lysine in the vacuole (Beckerich et al., 1986), which well explains why the cells could maintain high L-lysine levels over several days. In this regard, stored high L-lysine functioned as a reservoir of acetyl-CoA-based carbon, seemingly serving a purpose like that of a cellular lipid. The continuous degradation of the ketogenic amino acid during the stationary phase, inferred from the sustained intracellular abundance (Fig. 5C) and the activated catabolic pathway (Fig. 6A), continuously provided acetyl-CoA.

Isotopic tracer studies with 10 mM [$^{13}C_6$] L-lysine (Fig. 5C and D) and 10 mM [$^{13}C_6$] L-leucine (Fig. 5E and F) proved the efficient use of the two amino acids to form DHA. Based on ^{13}C enrichment, the external amino acids were the dominant sources to synthetize intracellular acetyl-CoA (up to 60% and 64%) and malonyl-CoA (up to 55% and 55%). During the first day after supplementation, newly formed DHA contained 34% of L-lysine-derived carbon, based on ^{13}C enrichment (Fig. 5D), whereas supplemented L-leucine accounted for 19% (Fig. 5F). The tracer study further revealed that both amino acids entered the TCA cycle, as inferred from the rapid incorporation of ^{13}C in succinyl-CoA (Fig. 5D and F). The slight incorporation of ^{13}C in PAL and OLE indicated that native fatty acid synthesis was still ongoing to some extent. Taken together, these results show that supplementation with ketogenic and mixed-type amino acids provided elevated levels of acetyl-CoA and malonyl-CoA, which, *inter alia,* boosted the production of PUFAs. In terms of production, the dilution of ^{13}C in DHA in both tracer cultures (Supplementary file 1, Fig. S8) indicated a diminishing contribution of the ketogenic amino acids during later stages of the process, suggesting sequential pulses for an intensified effect. Interesting differences between L-lysine and L-leucine resulted in ^{13}C labeling of the intracellular amino acid pools. Shortly after spiking [$^{13}C_6$] L-leucine into the culture, the intracellular L-leucine pool was found to be 95% ^{13}C-enriched, showing that it was almost completely composed of the externally added tracer. In contrast, the intracellular L-lysine pool revealed substantially lower ^{13}C enrichment upon [$^{13}C_6$] L-lysine addition. A possible explanation could be the distribution of intracellular L-lysine between the cytoplasm and the vacuole (Beckerich et al., 1986) so that only the cytosolic fraction was subjected to fast replenishment by the isotopic tracer. Such a compartmentation of L-lysine would also explain the observation that L-glutamate (being a high-abundance cytosolic amino acid) and other metabolites became more strongly enriched in ^{13}C than L-lysine itself (Fig. 5D).

3.8. Benchmarked in lab-scale bioreactors, a reduced nitrogen-to-carbon ratio helps limit the excretion of citrate in favor of DHA titer and selectivity

Additionally, we explored different media with varied ratios between carbon, nitrogen, and phosphorous to produce DHA, as the availability of these elements has a crucial impact on growth and fatty acid metabolism in *Y. lipolytica* (Blazeck et al., 2014). The variation in medium composition allowed for the creation of different types of nutrient limitations in shake flask cultures (Fig. 7). As compared to the reference process (Fig. 7A), doubling the amount of phosphate (Condition 2) resulted in 25% more DHA (125 mg L^{-1}) (Fig. 7B), while doubling the amount of carbon (Condition 3) increased the DHA titer even by 100% (250 mg L^{-1}) (Fig. 7C). The latter setup resulted in more citrate accumulation (up to 40 mM) and a higher biomass concentration. Therefore, an increased amount of glycerol was an efficient way to increase the production performance. Despite the differences in DHA production, however, the transcriptional changes of pathways associated with PUFA synthesis and central carbon metabolism were highly conserved between the different nutrient regimes (Fig. 7). Notably, the increased expression of genes encoding ketogenic amino acid pathways was observed for all tested nutrient conditions, suggesting a general response of the yeast to glycerol depletion (Fig. 7F) and promising a general boost of DHA production by enhanced ketogenic amino acid catabolism.

Next, we aimed to transfer the process to lab-scale bioreactors. Previously, only one process configuration was applied to overproduce DHA in *Y. lipolytica* Af4 in a bioreactor (Gemperlein et al., 2019). There, the set-up comprised a glycerol- or glucose-based fed-batch with continuous feeding of the corresponding carbon source after depletion of the initially batched amount. When using glycerol, this setup enabled the accumulation of 300 mg L^{-1} DHA over 300 h at a selectivity of 7% TFA, while cells reached a maximum biomass concentration of 30 g L^{-1} and formed citrate at up to 40 g L^{-1} during the glycerol-limited feed phase (Gemperlein et al., 2019). The selectivity of this process was much lower than that achieved in this work using glycerol-grown batch cultures in shake flasks (17% of TFA) (Fig. 1, Table 1), and the large amount of unused citrate at the end of the process was also a drawback.

We therefore decided to test different process alternatives. Given the positive effect of an increased glycerol level on the DHA titer (Figs. 1 and 7, Supplementary File 1, Fig. S3A), the first setup was comprised of a batch process with 100 g L^{-1} glycerol, 5 g L^{-1} $(NH_4)_2SO_4$, and 1 g L^{-1} KH_2PO_4 (C–N–P) (Fig. 8A). The online recording of process parameters revealed that the temperature and DO level were well controlled at the desired set-points, which was also the case for all other processes (Fig. 8). The final DHA titer (446 mg L^{-1}) was almost 50% higher than the value reported before, while the transiently accumulated citrate (58 mM) was reused completely (Gemperlein et al., 2019). Obviously, the setup that worked well in shake flasks could be successfully transferred to the bioreactor scale to overproduce DHA, and it was possible to increase the initial amount of carbon source to a higher level to generate higher titers. In contrast to the shake flask cultures, the accumulation of citrate was, however, much higher, likely caused by the higher initial glycerol level and the increased aeration. The selectivity of DHA production (9% of TFA) was rather low, caused by the elevated formation of native fatty acids (Table 4). In a second setup (C–N–2P), we reduced the C:P ratio and doubled the amount of phosphate, aiming at a higher biomass concentration (Fig. 8C). Indeed, cell growth lasted longer (even into the citrate consumption phase), and a significantly increased maximum biomass concentration (54 g L^{-1}) was reached after

Table 4
Benchmarking of ketogenic feeding strategies for DHA production in recombinant *Y. lipolytica* Af4. The data summarize the performance of batch and fed-batch processes in lab-scale bioreactors (Fig. 8). The basic batch medium contained 100 g L^{-1} of glycerol, 5 g L^{-1} of $(NH_4)_2SO_4$, and 1 g L^{-1} of KH_2PO_4 as sources for carbon (●), nitrogen (●), and phosphorous (●). Additional setups comprised double amounts of nitrogen (●●●●) and phosphorous (●●●●). Each configuration was operated as a batch process and as a fed-batch process, additionally supplemented during the stationary phase with two (●●) or three (●●●) feed pulses of L-lysine. The biomass concentration displays the maximum value achieved during the process. DHA titer, selectivity, and content reflect the maximum values at the process end, whereas the specific productivity represents the average over the entire process. The data display the average values and deviations from two biological replicates. Statistical significance was based on a paired *t*-test. CDM, cell dry mass; TFA, total fatty acids. Maximum numbers are given in bold.

	DHA titer [mg L^{-1}]	DHA selectivity [% of TFAs]	DHA yield [mg g_{CDM}^{-1}]	Biomass [g_{CDM} L^{-1}]	DHA productivity [mg L^{-1} d^{-1}]
C–N–P (●●●)	446 ± 49	9 ± 1	12 ± 1	38 ± 1	45 ± 6
C–N–P (●●●) L-Lysine (●●●)	809 ± 22 [a,b]	22 ± 0 [a]	22 ± 0	38 ± 1	90 ± 2 [a]
C–N–2P (●●●●)	574 ± 48	8 ± 0	11 ± 0	**54 ± 1**	64 ± 2
C–N–2P (●●●●) L-Lysine (●●●)	853 ± 54 [a,b]	21 ± 2 [a]	16 ± 1	**54 ± 1**	95 ± 6 [a]
C–2N–P (●●●●)	712 ± 46	16 ± 1	19 ± 3	40 ± 6	72 ± 5
C–2N–P (●●●●) L-Lysine (●●)	**1039 ± 63** [a,b]	**27 ± 1**	**24 ± 0**	43 ± 4	**106 ± 7** [a]

[a] Significantly enhanced by L-lysine feeding.
[b] Significantly enhanced compared to an assumed setup that received the same amount of carbon in the form glycerol, considering that the extra glycerol would proportionally increase DHA production.

approximately 150 h. Despite the higher cell concentration, it took much longer to re-consume the accumulated citrate. DHA accumulated to a final titer of 574 mg L^{-1}. In comparison to the reference process, the increased production was largely due to the higher level of cells. The ratio between biomass and DHA concentration was almost identical between the two processes, as was the DHA selectivity (8% of TFA) (Table 4). In a third set-up, we reduced the C:N ratio (C-2 N–P) by doubling the amount of nitrogen in the medium (Fig. 8C). This setup aimed to limit citrate overflow. It was inspired by the fact that citrate, although promoting the supply of acetyl-CoA, stimulated the generation of native fatty acids (Magdouli et al., 2020; Sabra et al., 2017) which competed with the formation of DHA, thereby causing a low selectivity for DHA production (Fig. 4A and B, Table 3). The excretion of citrate, *inter alia*, was known to be limited by a low C:N ratio (Goncalves et al., 2014). The chosen setup met all expectations. Citrate accumulated to a much lower extent (Fig. 8E), while the DHA titer (712 mg L^{-1}) and selectivity (16% of TFA) were found to be significantly increased (Table 4). Moreover, the cells grew much faster so that the maximum biomass concentration was reached one day earlier than that in the other processes. DHA production started approximately one day earlier as well (Fig. 8A, C, and E).

3.9. Benchmarking of the new L-lysine feeding strategy enables gram-scale production of DHA in Y. lipolytica Af4 in a fed-batch process

Finally, all three production conditions (C–N–P, C–N–2P, C–2N–P) were used to benchmark the newly developed feeding strategy at the bioreactor scale (Fig. 8B, D and F). L-Lysine was chosen as the supplement because it is an inexpensive industrial bulk product that is widely available from renewable feedstocks through microbial fermentation (Becker et al., 2011; Hoffmann et al., 2021). After the depletion of glycerol (after approximately 48 h), all cultures received a first shot of L-lysine. In the two nitrogen-limited cultures, the supplemented L-lysine was consumed at a high rate within only 24 h (Fig. 8D and E). Surprisingly, the presence of L-lysine in the process immediately stopped the excretion of citrate and even triggered its re-consumption, whereas citrate continued to increase in the corresponding non-supplemented processes (Fig. 8A, B, C, and D). Eventually, this phenomenon was caused by the nitrogen that was brought into the process through the amino acid. Over the next three days, *Y. lipolytica* Af4 consumed L-lysine (refilled in the culture *via* a second shot) with citrate, whereby the amino acid caused a massively increased citrate reassimilation rate. A third shot of L-lysine was given to both cultures after approximately 135 h. In contrast, the ammonium-enriched condition (C–2N–P) exhibited a more than threefold lower L-lysine uptake rate (Fig. 8F), so that, overall, only two pulses were given during the whole process. At the end of the process, the supplemented L-lysine was consumed in all three process setups.

Supplementation with the ketogenic amino acid L-lysine markedly boosted the DHA titer. The three supplemented cultures accumulated 809, 855, and 1039 mg L^{-1} DHA, respectively, 81%, 48% and 46% more than in the corresponding non-supplemented processes (Table 4). Beneficially, supplementation resulted in a significantly lower native fatty acid content, which drastically improved DHA selectivity to up to 27% of TFAs. It should be noted that L-lysine partially served as a carbon source for growth. Its addition slightly enhanced the biomass cell concentration compared to the non-supplemented cultures (Table 4). However, even when assuming that one would have added the same extra amount of carbon in the form of glycerol and this would have resulted in a concomitantly improved DHA titer, the feeding of L-lysine still appeared strongly superior (Table 4). DHA was formed at high selectivity (27% of TFA). Beneficially, the recombinant yeast did not produce any other twenty-two-carbon PUFAs such as DPA. Omega-3 and omega-6 DPA derivatives are typically found in microalgal and fish oils (Oh et al., 2020), where they account for up to 20% of the amount of DHA produced (Kujawska et al., 2021). Because of the high similarity to DHA, DPA derivatives are difficult to be separated away, adding extra costs to the downstream purification for high-value medical applications that require API-grade DHA (Yokochi et al., 1998). Therefore, *Y. lipolytica* Af4-based DPA-free DHA production might become an attractive route towards the medical markets.

Towards further improvement, our study suggests different genetic targets that could be implemented into the recombinant producer towards next generation cell factories. First, it appears promising to increase the synthesis of L-lysine and other ketogenic amino acids during the growth phase *via* the overexpression of feedback resistant biosynthetic enzymes and/or increase their degradation during the stationary phase. These changes could avoid extra costs that would result from external supplementation. Second, the expression of the PKS gene cluster should be amplified and extended to the growth phase. Strain Af4 did not express the cluster during the growth phase, likely causing the delayed product formation (Figs. 2 and 3). Eventually, this undesired feature was caused by the promoter minLEU2, a stationary-phase promoter, which was used to drive the cluster expression (Gemperlein et al., 2019). It seems straightforward to aim at re-designing the cluster for better expression dynamics, considering other promoters and, also, additional genetic control elements such as introns, upstream activating elements, spacers, and terminators, known to have huge effects on gene

expression in *Y. lipolytica* (Larroude et al., 2018; Schwartz et al., 2019; Wong et al., 2017). An earlier on-set of expression would allow to make use of the high abundance of acetyl-CoA and malonyl-CoA during the growth phase towards higher titers (Table 2). Third, genetic strategies that aim to elevate acetyl-CoA supply through the overexpression of *ACL* (Wei et al., 2021) and *ACC* (Tai and Stephanopoulos, 2013) appear promising to be tested. Fourth, the activation of lipid and fatty acid degradation appears as a relevant target. It could speed up the process, increase selectivity, and elevate CoA ester levels. Eventually, such efforts could follow orthogonal strategies to previous attempts that aimed at attenuating degradation (Niehus et al., 2018). Fifth, the role of the succinate dehydrogenase complex deserves to be studied further, given its strong up-regulation during the stationary phase (Fig. 3) and its potential impact on the generation of reactive oxygen species. In addition, our multi-omics data sets are freely available to be explored further in other directions. There seems still much to learn. For example, the function of about half of the hundred genes whose expression was most altered during production appeared entirely unknown (Supplementary material 1, Table S4).

In addition, the newly developed feeding strategy, could promote the production of other valuable chemicals in *Y. lipolytica*, including other CoA-based (polyunsaturated) fatty acids (Cao et al., 2022; Jia et al., 2022, 2023), polyketides, terpenoids, flavonoids, and tetracyclines (Choi and Da Silva, 2014; Sun et al., 2018b) whose synthesis is limited by CoA ester availability.

4. Conclusions

DHA is a marine PUFA of commercial value, given its multiple health benefits. A powerful strategy to overproduce DHA uses the recombinant strain *Y. lipolytica* Af4 which expresses a myxobacterial polyketide synthase (PKS)-like PUFA cluster (Gemperlein et al., 2019). Here, we provide a multi-omics view on the DHA production process in *Y. lipolytica* Af4. As shown, the shift from growth to the stationary phase at the onset of DHA production was associated to fundamental changes in global gene expression, involving the carbon core metabolic machinery (Fig. 3). Strikingly, the levels of the DHA precursors acetyl-CoA and malonyl-CoA dropped by up to 98% during the production phase (Fig. 2), linked to complex transcriptional changes of reactions involved in the formation and consumption of the two intermediates in various cellular compartments (Figs. 3 and 7). Hereby, we discovered that cells activated the degradation of ketogenic amino acids, contributing to the supply of acetyl-CoA (Fig. 6) which inspired to supplement these compounds to producing cultures. The strategy enabled gram scale DHA production in recombinant *Y. lipolytica* for the first time (Fig. 8, Table 5). The achieved titer was three-fold higher than before but still below industrial levels (Kujawska et al., 2021), leaving space for further improvement.

Strategically, PKS-based DHA production in *Y. lipolytica* displays an attractive route for the future. The use of the heterologous PUFA synthase offers a substantially reduced NADPH demand for DHA synthesis, as compared to artificially extended fatty acid biosynthetic pathways using heterologous elongases and desaturases (Gemperlein et al., 2019). Notably, elongase-desaturase-based *Y. lipolytica* strains have their strength in synthesizing smaller PFUAs, which does not require too extra many steps (Table 5). While, the application of this concept required huge efforts to synthesize the larger, twenty-carbon PUFA EPA, it failed to demonstrate high-efficiency DHA production (Xue et al., 2013). PKS-based routes might contribute to fill this gap in the future. As shown, our study takes a next step towards this goal.

Author statement

Sofija Jovanovic Gasovic, Demian Dietrich, Lars Gläser, Michael Kohlstedt, Pen Cao: investigation, formal analysis; Sofija Jovanovic Gasovic, Christoph Wittmann: visualization; Sofija Jovanovic Gasovic, Christoph Wittmann: drafting and revising the manuscript; Sofija Jovanovic Gasovic, Christoph Wittmann: design of study, conceptualization; Christoph Wittmann: supervision, editing, resources, funding acquisition.

Table 5
Production of omega-3 and omega-6 PUFAs between 18 and 22 carbons in length using different *Y. lipolytica* hosts and strategies. ALA: α-linolenic acid; ARA: arachidonic acid; DGLA: di-homo-γ-linolenic acid; DHA: docosahexaenoic acid; EPA: eicosapentanoic acid; GLA: γ-linolenic acid.

PUFA	Structure	Titer [mg L^{-1}]	Selectivity [% of TFAs]	Yield [mg g_{CDM}^{-1}]	Reference
DHA	C22:6 (ω-3)	**1040**	**27.3**	**24**	This work – L-lysine supplied
DHA	C22:6 (ω-3)	710	15.7	19	This work – non supplied
DHA	**DHA**	350	16.8	17	Gemperlein et al. (2019)
DHA	**DHA**	/	5.6	/	Xie et al. (2017)
EPA	C20:5 (ω-3)	/	56.0	222	Xie et al. (2017)
ARA	C20:4 (ω-6)	120	0.8	12	Liu et al. (2019b)
DGLA	C20:3 (ω-6)	160	0.8	/	Liu et al. (2017)
ALA	C18:3 (ω-3)	1400	17.0	70	Cordova and Alper (2018)
GLA	C18:3 (ω-6)	1780	9.0	/	Liu et al. (2017)

Data availability

Data will be made available on request.

5 Acknowledgments

Christoph Wittmann acknowledges financial support by the German Ministry for Education and Research (BMBF) through grants MYXO4PUFA (031B0346B) and MYXO4PUFA-2 (031B1049B) and by the German Research Foundation (DFG) through grant INST 256/418–1.

Appendix A. Supplementary data

Supplementary data to this article can be found online at https://doi.org/10.1016/j.ymben.2023.09.003.

References

Barth, G., 2013. *Yarrowia lipolytica*: Genetics, genomics, and physiology.
Barth, G., Gaillardin, C., 1997. Physiology and genetics of the dimorphic fungus *Yarrowia lipolytica*. FEMS Microbiol. Rev. 19, 219–237.
Bartosova, Z., Ertesvåg, H., Nyfløt, E.L., Kämpe, K., Aasen, I.M., Bruheim, P., 2021. Combined metabolome and lipidome analyses for in-depth characterization of lipid accumulation in the DHA producing *Aurantiochytrium* sp. T66. Metabolites 11, 135. https://doi.org/10.3390/metabo11030135.
Becker, J., Zelder, O., Haefner, S., Schröder, H., Wittmann, C., 2011. From zero to hero-Design-based systems metabolic engineering of *Corynebacterium glutamicum* for L-lysine production. Metab. Eng. 13, 159–168.
Beckerich, J.M., Lambert, M., Gaillardin, C., 1994. LYC1 is the structural gene for lysine N-6-acetyl transferase in yeast. Curr. Genet. 25, 24–29.
Beckerich, J.M., Pommies, E., Faivre, C., Lambert, M., Heslot, H., 1986. Estimation of compartmentation of lysine inside the cells of *Yarrowia lipolytica*. Biochimie 68, 517–529.
Belle, A., Tanay, A., Bitincka, L., Shamir, R., O'Shea, E.K., 2006. Quantification of protein half-lives in the budding yeast proteome. Proc. Natl. Acad. Sci. USA 103, 13004–13009.
Bellou, S., Makri, A., Triantaphyllidou, I.E., Papanikolaou, S., Aggelis, G., 2014. Morphological and metabolic shifts of *Yarrowia lipolytica* induced by alteration of the dissolved oxygen concentration in the growth environment. Microbiol. SEM 160, 807–817.
Beopoulos, A., Haddouche, R., Kabran, P., Dulermo, T., Chardot, T., Nicaud, J.M., 2012. Identification and characterization of DGA2, an acyltransferase of the DGAT1 acyl-CoA:diacylglycerol acyltransferase family in the oleaginous yeast *Yarrowia lipolytica*.

New insights into the storage lipid metabolism of oleaginous yeasts. Appl. Microbiol. Biotechnol. 93, 1523–1537.
Beopoulos, A., Mrozova, Z., Thevenieau, F., Le Dall, M.T., Hapala, I., Papanikolaou, S., Chardot, T., Nicaud, J.M., 2008. Control of lipid accumulation in the yeast *Yarrowia lipolytica*. Appl. Environ. Microbiol. 74, 7779–7789.
Bian, M.J., Li, S., Wei, H.H., Huang, S.P., Zhou, F., Zhu, Y.M., Zhu, G.P., 2018. Heteroexpression and biochemical characterization of a glucose 6-phosphate dehydrogenase from oleaginous yeast *Yarrowia lipolytica*. Protein Expr. Purif. 148, 1–8.
Biriukova, E.N., Medentsev, A.G., Arinbasarova, A., Akimenko, V.K., 2006. Tolerance of the yeast *Yarrowia lipolytica* to oxidative stress. Mikrobiologiia 75, 293–298.
Blazeck, J., Hill, A., Liu, L.Q., Knight, R., Miller, J., Pan, A., Otoupal, P., Alper, H.S., 2014. Harnessing *Yarrowia lipolytica* lipogenesis to create a platform for lipid and biofuel production. Nat. Commun. 5.
Bolten, C.J., Wittmann, C., 2008. Appropriate sampling for intracellular amino acid analysis in five phylogenetically different yeasts. Biotechnol. Lett. 30, 1993–2000.
Borkowska, M., Bialas, W., Celinska, E., 2020. A new set of reference genes for comparative gene expression analyses in *Yarrowia lipolytica*. FEMS Yeast Res. 20.
Calder, P.C., 2018. Very long-chain n-3 fatty acids and human health: fact, fiction and the future. Proc. Nutr. Soc. 77, 52–72.
Cao, L., Yin, M., Shi, T.Q., Lin, L., Ledesma-Amaro, R., Ji, X.J., 2022. Engineering *Yarrowia lipolytica* to produce nutritional fatty acids: current status and future perspectives. Synth Syst Biotechnol 7, 1024–1033.
Cardoso, C., Afonso, C., Bandarra, N.M., 2016. Dietary DHA and health: cognitive function ageing. Nutr. Res. Rev. 29, 281–294.
Carsanba, E., Papanikolaou, S., Fickers, P., Erten, H., 2020. Lipids by *Yarrowia lipolytica* strains cultivated on glucose in batch cultures. Microorganisms 8.
Castro, L.F., Tocher, D.R., Monroig, O., 2016. Long-chain polyunsaturated fatty acid biosynthesis in chordates: insights into the evolution of Fads and Elovl gene repertoire. Prog. Lipid Res. 62, 25–40.
Cavallo, E., Charreau, H., Cerrutti, P., Foresti, M.L., 2017. *Yarrowia lipolytica*: a model yeast for citric acid production. FEMS Yeast Res. 17.
Chen, H., He, X., Geng, H., Liu, H., 2014. Physiological characterization of ATP-citrate lyase in *Aspergillus niger*. J. Ind. Microbiol. Biotechnol. 41, 721–731.
Choi, J.W., Da Silva, N.A., 2014. Improving polyketide and fatty acid synthesis by engineering of the yeast acetyl-CoA carboxylase. J. Biotechnol. 187, 56–59.
Colombo, S.M., Rodgers, T.F.M., Diamond, M.L., Bazinet, R.P., Arts, M.T., 2020. Projected declines in global DHA availability for human consumption as a result of global warming. Ambio 49, 865–880.
Cordova, L.T., Alper, H.S., 2018. Production of alpha-linolenic acid in *Yarrowia lipolytica* using low-temperature fermentation. Appl. Microbiol. Biotechnol. 102, 8809–8816.
Cui, Z.Y., Gao, C.J., Li, J.J., Hou, J., Lin, C.S.K., Qi, Q.S., 2017. Engineering of unconventional yeast *Yarrowia lipolytica* for efficient succinic acid production from glycerol at low pH. Metab. Eng. 42, 126–133.
D'Andrea, G., 2000. Classifying amino acids as gluco(glyco)genic, ketogenic, or both. Biochem. Educ. 28, 27–28.
da Silva, L.V., Coelho, M.A.Z., da Silva, M.R.S., Amaral, P.F.F., 2020. Investigation of mitochondrial protein expression profiles of *Yarrowia lipolytica* in response to citric acid production. Bioproc. Biosyst. Eng. 43, 1703–1715.
Dujon, B., Sherman, D., Fischer, G., Durrens, P., Casaregola, S., Lafontaine, I., De Montigny, J., Marck, C., Neuveglise, C., Talla, E., Goffard, N., Frangeul, L., Aigle, M., Anthouard, V., Babour, A., Barbe, V., Barnay, S., Blanchin, S., Beckerich, J.M., Beyne, E., Bleykasten, C., Boisrame, A., Boyer, J., Cattolico, L., Confanioleri, F., De Daruvar, A., Despons, L., Fabre, E., Fairhead, C., Ferry-Dumazet, H., Groppi, A., Hantraye, F., Hennequin, C., Jauniaux, N., Joyet, P., Kachouri, R., Kerrest, A., Koszul, R., Lemaire, M., Lesur, I., Ma, L., Muller, H., Nicaud, J.M., Nikolski, M., Oztas, S., Ozier-Kalogeropoulos, O., Pellenz, S., Potier, S., Richard, G.F., Straub, M. L., Suleau, A., Swennen, D., Tekaia, F., Wesolowski-Louvel, M., Westhof, E., Wirth, B., Zeniou-Meyer, M., Zivanovic, I., Bolotin-Fukuhara, M., Thierry, A., Bouchier, C., Caudron, B., Scarpelli, C., Gaillardin, C., Weissenbach, J., Wincker, P., Souciet, J.L., 2004. Genome evolution in yeasts. Nature 430, 35–44.
Dulermo, R., Gamboa-Melendez, H., Ledesma-Amaro, R., Thevenieau, F., Nicaud, J.M., 2015. Unraveling fatty acid transport and activation mechanisms in *Yarrowia lipolytica*. Biochim. Biophys. Acta 1851, 1202–1217.
Dulermo, T., Nicaud, J.M., 2011. Involvement of the G3P shuttle and beta-oxidation pathway in the control of TAG synthesis and lipid accumulation in *Yarrowia lipolytica*. Metab. Eng. 13, 482–491.
Egermeier, M., Russmayer, H., Sauer, M., Marx, H., 2017. Metabolic flexibility of *Yarrowia lipolytica* growing on glycerol. Front. Microbiol. 8, 49.
Emery, J.A., Norambuena, F., Trushenski, J., Turchini, G.M., 2016. Uncoupling EPA and DHA in fish nutrition: dietary demand is limited in Atlantic salmon and effectively met by DHA alone. Lipids 51, 399–412.
Erian, A.M., Egermeier, M., Marx, H., Sauer, M., 2022. Insights into the glycerol transport of *Yarrowia lipolytica*. Yeast 39, 323–336.
Frick, O., Wittmann, C., 2005. Characterization of the metabolic shift between oxidative and fermentative growth in *Saccharomyces cerevisiae* by comparative ^{13}C flux analysis. Microb. Cell Factories 4.
Gatter, M., Ottlik, S., Kovesi, Z., Bauer, B., Matthaus, F., Barth, G., 2016. Three alcohol dehydrogenase genes and one acetyl-CoA synthetase gene are responsible for ethanol utilization in *Yarrowia lipolytica*. Fungal Genet. Biol. 95, 30–38.
Gemperlein, K., Dietrich, D., Kohlstedt, M., Zipf, G., Bernauer, H.S., Wittmann, C., Wenzel, S.C., Müller, R., 2019. Polyunsaturated fatty acid production by *Yarrowia lipolytica* employing designed myxobacterial PUFA synthases. Nat. Commun. 10, 4055.
Gemperlein, K., Rachid, S., Garcia, R.O., Wenzel, S.C., Müller, R., 2014. Polyunsaturated fatty acid biosynthesis in myxobacteria: different PUFA synthases and their product diversity. Chem. Sci. 5, 1733–1741.
Gläser, L., Kuhl, M., Jovanovic, S., Fritz, M., Vögeli, B., Erb, T.J., Becker, J., Wittmann, C., 2020. A common approach for absolute quantification of short chain CoA thioesters in prokaryotic and eukaryotic microbes. Microb. Cell Factories 19, 160.
Gläser, L., Kuhl, M., Stegmüller, J., Rückert, C., Myronovskyi, M., Kalinowski, J., Luzhetskyy, A., Wittmann, C., 2021. Superior production of heavy pamamycin derivatives using a bkdR deletion mutant of *Streptomyces albus* J1074/R2. Microb. Cell Factories 20, 111.
Goncalves, F.A., Colen, G., Takahashi, J.A., 2014. *Yarrowia lipolytica* and its multiple applications in the biotechnological industry. Sci. World J. 2014, 476207.
Grigoriev, I.V., Nikitin, R., Haridas, S., Kuo, A., Ohm, R., Otillar, R., Riley, R., Salamov, A., Zhao, X.L., Korzeniewski, F., Smirnova, T., Nordberg, H., Dubchak, I., Shabalov, I., 2014. MycoCosm portal: gearing up for 1000 fungal genomes. Nucleic Acids Res. 42, D699–D704.
Guo, H.W., Madzak, C., Du, G.C., Zhou, J.W., Chen, J., 2014. Effects of pyruvate dehydrogenase subunits overexpression on the α-ketoglutarate production in *Yarrowia lipolytica* WSH-Z06. Appl. Microbiol. Biotechnol. 98, 7003–7012.
Guzzo, G., Sciacovelli, M., Bernardi, P., Rasola, A., 2014. Inhibition of succinate dehydrogenase by the mitochondrial chaperone TRAP1 has anti-oxidant and anti-apoptotic effects on tumor cells. Oncotarget 5, 11897–11908.
Haddouche, R., Poirier, Y., Delessert, S., Sabirova, J., Pagot, Y., Neuveglise, C., Nicaud, J. M., 2011. Engineering polyhydroxyalkanoate content and monomer composition in the oleaginous yeast *Yarrowia lipolytica* by modifying the ss-oxidation multifunctional protein. Appl. Microbiol. Biotechnol. 91, 1327–1340.
Heggeset, TMB, Ertesvåg, H, Liu, B, Ellingsen, TE, Vadstein, O, Aasen, IM, 2019. Lipid and DHA-production in *Aurantiochytrium* sp. - Responses to nitrogen starvation and oxygen limitation revealed by analyses of production kinetics and global transcriptomes. Sci Rep. 9 (1), 19470. https://doi.org/10.1038/s41598-019-55902-4. PMID: 31857635; PMCID: PMC6923395.
Hicks, C.C., Cohen, P.J., Graham, N.A.J., Nash, K.L., Allison, E.H., D'Lima, C., Mills, D.J., Roscher, M., Thilsted, S.H., Thorne-Lyman, A.L., MacNeil, M.A., 2019. Harnessing global fisheries to tackle micronutrient deficiencies. Nature 574, 95–98.
Hixson, S.M., Arts, M.T., 2016. Climate warming is predicted to reduce omega-3, long-chain, polyunsaturated fatty acid production in phytoplankton. Global Change Biol. 22, 2744–2755.
Hoffmann, S.L., Kohlstedt, M., Jungmann, L., Hutter, M., Poblete-Castro, I., Becker, J., Wittmann, C., 2021. Cascaded valorization of brown seaweed to produce l-lysine and value-added products using *Corynebacterium glutamicum* streamlined by systems metabolic engineering. Metab. Eng. 67, 293–307.
Holz, M., Forster, A., Mauersberger, S., Barth, G., 2009. Aconitase overexpression changes the product ratio of citric acid production by *Yarrowia lipolytic*a. Appl. Microbiol. Biotechnol. 81, 1087–1096.
Holz, M., Otto, C., Kretzschmar, A., Yovkova, V., Aurich, A., Potter, M., Marx, A., Barth, G., 2011. Overexpression of alpha-ketoglutarate dehydrogenase in Yarrowia lipolytica and its effect on production of organic acids. Appl. Microbiol. Biotechnol. 89, 1519–1526.
Huang, S., Millar, A.H., 2013. Succinate dehydrogenase: the complex roles of a simple enzyme. Curr. Opin. Plant Biol. 16, 344–349.
Hussain, S.A., Sarker, M.I., Yosief, H.O., Yadav, M.P., 2021. Evaluation of diverse biochemical stimulants to enhance growth, lipid and docosahexaenoic acid (DHA) production of *Aurantiochytrium* sp. ATCC PRA-276. Biocatal. Agric. Biotechnol. 36.
Imatoukene, N., Verbeke, J., Beopoulos, A., Taghki, A.I., Thomasset, B., Sarde, C.O., Nonus, M., Nicaud, J.M., 2017. A metabolic engineering strategy for producing conjugated linoleic acids using the oleaginous yeast *Yarrowia lipolytica*. Appl. Microbiol. Biotechnol. 101, 4605–4616.
Jaishankar, J., Srivastava, P., 2017. Molecular basis of stationary phase survival and applications. Front. Microbiol. 8, 2000.
Ji, X.J., Huang, H., 2019. Engineering microbes to produce polyunsaturated fatty acids. Trends Biotechnol. 37, 344–346.
Jia, Y.L., Du, F., Nong, F.T., Li, J., Huang, P.W., Ma, W., Gu, Y., Sun, X.M., 2023. Function of the polyketide synthase domains of *Schizochytrium* sp. on fatty acid synthesis in *Yarrowia lipolytica*. J. Agric. Food Chem. 2446–2454.
Jia, Y.L., Wang, L.R., Zhang, Z.X., Gu, Y., Sun, X.M., 2022. Recent advances in biotechnological production of polyunsaturated fatty acids by *Yarrowia lipolytica*. Crit. Rev. Food Sci. Nutr. 62, 8920–8934.
Jovanovic, S., Dietrich, D., Becker, J., Kohlstedt, M., Wittmann, C., 2021. Microbial production of polyunsaturated fatty acids - high-value ingredients for aquafeed, superfoods, and pharmaceuticals. Curr. Opin. Biotechnol. 69, 199–211.
Kabeya, N., Fonseca, M.M., Ferrier, D.E.K., Navarro, J.C., Bay, L.K., Francis, D.S., Tocher, D.R., Castro, L.F.C., Monroig, O., 2018. Genes for de novo biosynthesis of omega-3 polyunsaturated fatty acids are widespread in animals. Sci. Adv. 4, eaar6849.
Kamzolova, S.V., Lunina, J.N., Morgunov, I.G., 2011. Biochemistry of citric acid production from rapeseed oil by *Yarrowia lipolytica* yeast. J. Am. Oil Chem. Soc. 88, 1965–1976.
Kiel, J.A., Veenhuis, M., van der Klei, I.J., 2006. PEX genes in fungal genomes: common, rare or redundant. Traffic 7, 1291–1303.
Kind, S., Neubauer, S., Becker, J., Yamamoto, M., Völkert, M., Abendroth, G.V., Zelder, O., Wittmann, C., 2014. From zero to hero - production of bio-based nylon from renewable resources using engineered *Corynebacterium glutamicum*. Metab. Eng. 25, 113–123.
Kohlstedt, M., Weimer, A., Weiland, F., Stolzenberger, J., Selzer, M., Sanz, M., Kramps, L., Wittmann, C., 2022. Biobased PET from lignin using an engineered cis,

cis-muconate-producing *Pseudomonas putida* strain with superior robustness, energy and redox properties. Metab. Eng. 72, 337–352.
Kohlstedt, M., Wittmann, C., 2019. GC-MS-based ^{13}C metabolic flux analysis resolves the parallel and cyclic glucose metabolism of *Pseudomonas putida* KT2440 and *Pseudomonas aeruginosa* PAO1. Metab. Eng. 54, 35–53.
Krink-Koutsoubelis, N., Loechner, A.C., Lechner, A., Link, H., Denby, C.M., Vogeli, B., Erb, T.J., Yuzawa, S., Jakociunas, T., Katz, L., Jensen, M.K., Sourjik, V., Keasling, J. D., 2018. Engineered production of short-chain acyl-Coenzyme A esters in *Saccharomyces cerevisiae*. ACS Synth. Biol. 7, 1105–1115.
Krömer, J.O., Fritz, M., Heinzle, E., Wittmann, C., 2005. In vivo quantification of intracellular amino acids and intermediates of the methionine pathway in *Corynebacterium glutamicum*. Anal. Biochem. 340, 171–173.
Kujawska, N., Talbierz, S., Debowski, M., Kazimierowicz, J., Zielinski, M., 2021. Cultivation method effect on *Schizochytrium* sp. biomass growth and docosahexaenoic acid (DHA) production with the use of waste glycerol as a source of organic carbon. Energies 14.
Lange, A., Becker, J., Schulze, D., Cahoreau, E., Portais, J.C., Haefner, S., Schröder, H., Krawczyk, J., Zelder, O., Wittmann, C., 2017. Bio-based succinate from sucrose: high-resolution ^{13}C metabolic flux analysis and metabolic engineering of the rumen bacterium *Basfia succiniciproducens*. Metab. Eng. 44, 198–212.
Larroude, M., Rossignol, T., Nicaud, J.M., Ledesma-Amaro, R., 2018. Synthetic biology tools for engineering *Yarrowia lipolytica*. Biotechnol. Adv. 36, 2150–2164.
Li, Q., Bai, Z., O'Donnell, A., Harvey, L.M., Hoskisson, P.A., McNeil, B., 2011. Oxidative stress in fungal fermentation processes: the roles of alternative respiration. Biotechnol. Lett. 33, 457–467.
Li, X., Wang, P., Ge, Y.D., Wang, W., Abbas, A., Zhu, G.P., 2013. $NADP^+$-specific isocitrate dehydrogenase from oleaginous yeast *Yarrowia lipolytica* CLIB122: biochemical characterization and coenzyme sites evaluation. Appl. Biochem. Biotechnol. 171, 403–416.
Liu, H., Marsafari, M., Deng, L., Xu, P., 2019a. Understanding lipogenesis by dynamically profiling transcriptional activity of lipogenic promoters in *Yarrowia lipolytica*. Appl. Microbiol. Biotechnol. 103, 3167–3179.
Liu, H., Song, Y., Fan, X., Wang, C., Lu, X., Tian, Y., 2020. *Yarrowia lipolytica* as an oleaginous platform for the production of value-added fatty acid-based bioproducts. Front. Microbiol. 11, 608662.
Liu, H.H., Madzak, C., Sun, M.L., Ren, L.J., Song, P., Huang, H., Ji, X.J., 2017. Engineering *Yarrowia lipolytica* for arachidonic acid production through rapid assembly of metabolic pathway. Biochem. Eng. J. 119, 52–58.
Liu, H.H., Wang, C., Lu, X.Y., Huang, H., Tian, Y., Ji, X.J., 2019b. Improved production of arachidonic acid by combined pathway engineering and synthetic enzyme fusion in *Yarrowia lipolytica*. J. Agric. Food Chem. 67, 9851–9857.
Liu, N., Qiao, K., Stephanopoulos, G., 2016. ^{13}C Metabolic flux analysis of acetate conversion to lipids by *Yarrowia lipolytica*. Metab. Eng. 38, 86–97.
Lorenz, M.C., Fink, G.R., 2001. The glyoxylate cycle is required for fungal virulence. Nature 412, 83–86.
Lubuta, P., Workman, M., Kerkhoven, E.J., Workman, C.T., 2019. Investigating the influence of glycerol on the utilization of glucose in *Yarrowia lipolytica* using RNA-seq-based transcriptomics. G3 (Bethesda) 9, 4059–4071.
Luevano, L.A., Moyano, E., de Lacoba, M.G., Rial, E., Uribe-Carvajal, S., 2010. Identification of the mitochondrial carrier that provides *Yarrowia lipolytica* with a fatty acid- induced and nucleotides-sensitive uncoupling protein-like activity. Biophys. J. 98, 736a-736a.
Lundebye, A.K., Lock, E.J., Rasinger, J.D., Nostbakken, O.J., Hannisdal, R., Karlsbakk, E., Wennevik, V., Madhun, A.S., Madsen, L., Graff, I.E., Ornsrud, R., 2017. Lower levels of persistent organic pollutants, metals and the marine omega 3-fatty acid DHA in farmed compared to wild Atlantic salmon (Salmo salar). Environ. Res. 155, 49–59.
Magdouli, S., Guedri, T., Rouissi, T., Brar, S.K., Blais, J.F., 2020. Sync between leucine, biotin and citric acid to improve lipid production by *Yarrowia lipolytic*a on crude glycerol-based media, Vol. 142. Biomass Bioenerg. 105764.
Martin-Perez, M., Villén, J., 2017. Determinants and regulation of protein turnover in yeast. Cell Syst 5, 283–294 e5.
Mlickova, K., Luo, Y., d'Andrea, S., Pec, P., Chardot, T., Nicaud, J.M., 2004. Acyl-CoA oxidase, a key step for lipid accumulation in the yeast *Yarrowia lipolytica*. J. Mol. Catal. B Enzym. 28, 81–85.
Mun, J.G., Legette, L.L., Ikonte, C.J., Mitmesser, S.H., 2019. Choline and DHA in maternal and infant nutrition: synergistic implications in brain and eye health. Nutrients 11.
Nazir, Y., Shuib, S., Kalil, M.S., Song, Y.D., Hamid, A.A., 2018. Optimization of culture conditions for enhanced growth, lipid and docosahexaenoic acid (DHA) production of *Aurantiochytrium* SW1 by response surface methodology. Sci. Rep. 8.
Niehus, X., Crutz-Le Coq, A.-M., Sandoval, G., Nicaud, J.-M., Ledesma-Amaro, R., 2018. Engineering *Yarrowia lipolytica* to enhance lipid production from lignocellulosic materials. Biotechnol. Biofuels 11, 11.
Oh, C.-E., Kim, G.-J., Park, S.-J., Choi, S., Park, M.-J., Lee, O.M., Seo, J.-W., Son, H.-J., 2020. Purification of high purity docosahexaenoic acid from *Schizochytrium* sp. SH103 using preparative-scale HPLC. Applied Biological Chemistry 63, 56.
Papanikolaou, S., Aggelis, G., 2003. Modeling lipid accumulation and degradation in *Yarrowia lipolytica* cultivated on industrial fats. Curr. Microbiol. 46, 398–402.
Park, S.J., Tseng, C.P., Gunsalus, R.P., 1995. Regulation of succinate dehydrogenase (sdhCDAB) operon expression in *Escherichia coli* in response to carbon supply and anaerobiosis: role of ArcA and Fnr. Mol. Microbiol. 15, 473–482.
Park, Y.K., Ledesma-Amaro, R., Nicaud, J.M., 2020. De novo biosynthesis of odd-chain fatty acids in *Yarrowia lipolytica* enabled by modular pathway engineering. Front. Bioeng. Biotechnol. 7.
Pauli, S., Kohlstedt, M., Lamber, J., Weiland, F., Becker, J., Wittmann, C., 2023. Systems metabolic engineering upgrades *Corynebacterium glutamicum* for selective high-level production of the chiral drug precursor and cell-protective extremolyte L-pipecolic acid. Metab. Eng. 77, 100–117.
Pei, G.S., Li, X.R., Liu, L.S., Liu, J., Wang, F.Z., Chen, L., Zhang, W.W., 2017. De novo transcriptomic and metabolomic analysis of docosahexaenoic acid (DHA)-producing *Crypthecodinium cohnii* during fed-batch fermentation. Algal Res. 26, 380–391.
Pomraning, K.R., Bredeweg, E.L., Kerkhoven, E.J., Barry, K., Haridas, S., Hundley, H., LaButti, K., Lipzen, A., Yan, M., Magnuson, J.K., Simmons, B.A., Grigoriev, I.V., Nielsen, J., Baker, S.E., 2018. Regulation of yeast-to-hyphae transition in *Yarrowia lipolytica*. mSphere 3.
Pomraning, K.R., Kim, Y.M., Nicora, C.D., Chu, R.K., Bredeweg, E.L., Purvine, S.O., Hu, D., Metz, T.O., Baker, S.E., 2016. Multi-omics analysis reveals regulators of the response to nitrogen limitation in *Yarrowia lipolytica*. BMC Genom. 17, 138.
Qiao, K, Imam Abidi, SH, Liu, H, Zhang, H, Chakraborty, S, Watson, N, Kumaran Ajikumar, P, Stephanopoulos, G, 2015. Engineering lipid overproduction in the oleaginous yeast *Yarrowia lipolytica*. Metab Eng 29, 56–65. https://doi.org/10.1016/j.ymben.2015.02.005. Epub 2015 Feb 27. PMID: 25732624.
Rodriguez, G.M., Hussain, M.S., Gambill, L., Gao, D., Yaguchi, A., Blenner, M., 2016. Engineering xylose utilization in *Yarrowia lipolytica* by understanding its cryptic xylose pathway. Biotechnol. Biofuels 9, 149.
Rohles, C., Pauli, S., Giesselmann, G., Kohlstedt, M., Becker, J., Wittmann, C., 2022. Systems metabolic engineering of *Corynebacterium glutamicum* eliminates all by-products for selective and high-yield production of the platform chemical 5-aminovalerate. Metab. Eng. 73, 168–181.
Rohles, C.M., Gläser, L., Kohlstedt, M., Giesselmann, G., Pearson, S., del Campo, A., Becker, J., Wittmann, C., 2018. A bio-based route to the carbon-5 chemical glutaric acid and to bionylon-6,5 using metabolically engineered Corynebacterium glutamicum. Green Chem. 20, 4662–4674.
Sabra, W., Bommareddy, R.R., Maheshwari, G., Papanikolaou, S., Zeng, A.P., 2017. Substrates and oxygen dependent citric acid production by *Yarrowia lipolytica*: insights through transcriptome and fluxome analyses. Microb. Cell Factories 16, 78.
Sahin, D., Tas, E., Altindag, U.H., 2018. Enhancement of docosahexaenoic acid (DHA) production from *Schizochytrium* sp. S31 using different growth medium conditions. Amb. Express 8, 7.
Santin, O., Moncalian, G., 2018. Loading of malonyl-CoA onto tandem acyl carrier protein domains of polyunsaturated fatty acid synthases. J. Biol. Chem. 293, 12491–12501.
Schwartz, C., Cheng, J.F., Evans, R., Schwartz, C.A., Wagner, J.M., Anglin, S., Beitz, A., Pan, W., Lonardi, S., Blenner, M., Alper, H.S., Yoshikuni, Y., Wheeldon, I., 2019. Validating genome-wide CRISPR-Cas9 function improves screening in the oleaginous yeast *Yarrowia lipolytica*. Metab. Eng. 55, 102–110.
Schwechheimer, S.K., Becker, J., Peyriga, L., Portais, J.C., Sauer, D., Müller, R., Hoff, B., Haefner, S., Schröder, H., Zelder, O., Wittmann, C., 2018a. Improved riboflavin production with *Ashbya gossypii* from vegetable oil based on ^{13}C metabolic network analysis with combined labeling analysis by GC/MS, LC/MS, 1D, and 2D NMR. Metab. Eng. 47, 357–373.
Schwechheimer, S.K., Becker, J., Peyriga, L., Portais, J.C., Wittmann, C., 2018b. Metabolic flux analysis in Ashbya gossypii using (13)C-labeled yeast extract: industrial riboflavin production under complex nutrient conditions. Microb. Cell Factories 17, 162.
Shaigani, P., Awad, D., Redai, V., Fuchs, M., Haack, M., Mehlmer, N., Brueck, T., 2021. Oleaginous yeasts- substrate preference and lipid productivity: a view on the performance of microbial lipid producers. Microb. Cell Factories 20, 220.
Shao, D., Villet, O., Zhang, Z., Choi, S.W., Yan, J., Ritterhoff, J., Gu, H.W., Djukovic, D., Christodoulou, D., Kolwicz, S.C., Raftery, D., Tian, R., 2018. Glucose promotes cell growth by suppressing branched-chain amino acid degradation. Nat. Commun. 9.
Sun, G.Y., Simonyi, A., Fritsche, K.L., Chuang, D.Y., Hannink, M., Gu, Z., Greenlief, C.M., Yao, J.K., Lee, J.C., Beversdorf, D.Q., 2018a. Docosahexaenoic acid (DHA): an essential nutrient and a nutraceutical for brain health and diseases. Prostaglandins Leukot. Essent. Fatty Acids 136, 3–13.
Sun, T., Li, S.B., Song, X.Y., Pei, G.S., Diao, J.J., Cui, J.Y., Shi, M.L., Chen, L., Zhang, W. W., 2018b. Re-direction of carbon flux to key precursor malonyl-CoA via artificial small RNAs in photosynthetic *Synechocystis* sp. PCC 6803. Biotechnol. Biofuels 11.
Swanson, D., Block, R., Mousa, S.A., 2012. Omega-3 fatty acids EPA and DHA: health benefits throughout life. Adv. Nutr. 3, 1–7.
Tai, M., Stephanopoulos, G., 2013. Engineering the push and pull of lipid biosynthesis in oleaginous yeast *Yarrowia lipolytica* for biofuel production. Metab. Eng. 15, 1–9.
Theron, C.W., Vandermies, M., Telek, S., Steels, S., Fickers, P., 2020. Comprehensive comparison of *Yarrowia lipolytica* and *Pichia pastoris* for production of *Candida antarctica* lipase B. Sci. Rep. 10, 1741.
Thevenieau, F., Le Dall, M.T., Nthangeni, B., Mauersberger, S., Marchal, R., Nicaud, J.M., 2007. Characterization of *Yarrowia lipolytica* mutants affected in hydrophobic substrate utilization. Fungal Genet. Biol. 44, 531–542.
Trebulle, P., Nicaud, J.M., Leplat, C., Elati, M., 2017. Inference and interrogation of a coregulatory network in the context of lipid accumulation in *Yarrowia lipolytica*. NPJ Syst Biol Appl 3, 21.
Valenzuela, A., Nieto, M.S., 2001. Docosahexaenoic acid (DHA) in fetal development and in infant nutrition. Rev. Med. Chile 129, 1203–1211.
van Winden, W.A., Wittmann, C., Heinzle, E., Heijnen, J.J., 2002. Correcting mass isotopomer distributions for naturally occurring isotopes. Biotechnol. Bioeng. 80, 477–479.
Vorapreeda, T., Thammarongtham, C., Cheevadhanarak, S., Laoteng, K., 2012. Alternative routes of acetyl-CoA synthesis identified by comparative genomic analysis: involvement in the lipid production of oleaginous yeast and fungi. Microbiology 158, 217–228.

Wan, X., Peng, Y.F., Zhou, X.R., Gong, Y.M., Huang, F.H., Moncalian, G., 2016. Effect of cerulenin on fatty acid composition and gene expression pattern of DHA-producing strain *Colwellia psychrerythraea* strain 34H. Microb. Cell Factories 15, 30.

Wang, K.F., Shi, T.Q., Lin, L., Wei, P., Ledesma-Amaro, R., Ji, X.J., 2022. Engineering *Yarrowia lipolytica* to produce tailored chain-length fatty acids and their derivatives. ACS Synth. Biol. 11, 2564–2577.

Wang, Y., Liu, C.L., Storey, J.D., Tibshirani, R.J., Herschlag, D., Brown, P.O., 2002. Precision and functional specificity in mRNA decay. Proc. Natl. Acad. Sci. U.S.A. 99, 5860–5865.

Wang, Z., Wang, D.H., Park, H.G., Tobias, H.J., Kothapalli, K.S.D., Brenna, J.T., 2019. Structural identification of monounsaturated branched chain fatty acid methyl esters by combination of electron ionization and covalent adduct chemical ionization tandem mass spectrometry. Anal. Chem. 91, 15147–15154.

Wasylenko, T.M., Ahn, W.S., Stephanopoulos, G., 2015. The oxidative pentose phosphate pathway is the primary source of NADPH for lipid overproduction from glucose in *Yarrowia lipolytica*. Metab. Eng. 30, 27–39.

Wei, H., Wang, W., Knoshaug, E.P., Chen, X.W., Van Wychen, S., Bomble, Y.J., Himmel, M.E., Zhang, M., 2021. Disruption of the Snf1 gene enhances cell growth and reduces the metabolic burden in cellulase-expressing and lipid-accumulating Yarrowia lipolytica. Front. Microbiol. 12.

Weiland, F., Barton, N., Kohlstedt, M., Becker, J., Wittmann, C., 2023. Systems metabolic engineering upgrades *Corynebacterium glutamicum* to high-efficiency *cis, cis*-muconic acid production from lignin-based aromatics. Metab. Eng. 75, 153–169.

Wittmann, C., 2007. Fluxome analysis using GC-MS. Microb. Cell Factories 6, 6.

Wittmann, C., Krömer, J.O., Kiefer, P., Binz, T., Heinzle, E., 2004. Impact of the cold shock phenomenon on quantification of intracellular metabolites in bacteria. Anal. Biochem. 327, 135–139.

Wong, L., Engel, J., Jin, E., Holdridge, B., Xu, P., 2017. YaliBricks, a versatile genetic toolkit for streamlined and rapid pathway engineering in *Yarrowia lipolytica*. Metab Eng Commun 5, 68–77.

Woolfson, A.M.J., 1983. Amino acids - their role as an energy-source. Proc. Nutr. Soc. 42, 489–495.

Xie, D., Miller, E., Sharpe, P., Jackson, E., Zhu, Q., 2017. Omega-3 production by fermentation of *Yarrowia lipolytica*: from fed-batch to continuous. Biotechnol. Bioeng. 114, 798–812.

Xu, P., Qiao, K.J., Stephanopoulos, G., 2017. Engineering oxidative stress defense pathways to build a robust lipid production platform in *Yarrowia lipolytica*. Biotechnol. Bioeng. 114, 1521–1530.

Xue, Z., Sharpe, P.L., Hong, S.P., Yadav, N.S., Xie, D., Short, D.R., Damude, H.G., Rupert, R.A., Seip, J.E., Wang, J., Pollak, D.W., Bostick, M.W., Bosak, M.D., Macool, D.J., Hollerbach, D.H., Zhang, H., Arcilla, D.M., Bledsoe, S.A., Croker, K., McCord, E.F., Tyreus, B.D., Jackson, E.N., Zhu, Q., 2013. Production of omega-3 eicosapentaenoic acid by metabolic engineering of *Yarrowia lipolytica*. Nat. Biotechnol. 31, 734–740.

Yanai, H., Masui, Y., Katsuyama, H., Adachi, H., Kawaguchi, A., Hakoshima, M., Waragai, Y., Harigae, T., Sako, A., 2018. An improvement of cardiovascular risk factors by omega-3 polyunsaturated fatty acids. J. Clin. Med. Res. 10, 281–289.

Yokochi, T., Honda, D., Higashihara, T., Nakahara, T., 1998. Optimization of docosahexaenoic acid production by *Schizochytrium limacinum* SR21. Appl. Microbiol. Biotechnol. 49, 72–76.

Yuzbasheva, E.Y., Agrimi, G., Yuzbashev, T.V., Scarcia, P., Vinogradova, E.B., Palmieri, L., Shutov, A.V., Kosikhina, I.M., Palmieri, F., Sineoky, S.P., 2019. The mitochondrial citrate carrier in *Yarrowia lipolytica*: its identification, characterization and functional significance for the production of citric acid. Metab. Eng. 54, 264–274.

Yuzbasheva, E.Y., Mostova, E.B., Andreeva, N.I., Yuzbashev, T.V., Laptev, I.A., Sobolevskaya, T.I., Sineoky, S.P., 2017. Co-expression of glucose-6-phosphate dehydrogenase and acyl-CoA binding protein enhances lipid accumulation in the yeast *Yarrowia lipolytica*. N. Biotech. 39, 18–21.

Zhang, T.T., Xu, J., Wang, Y.M., Xue, C.H., 2019. Health benefits of dietary marine DHA/EPA-enriched glycerophospholipids. Prog. Lipid Res. 75, 100997.